

1 **Influence of bank slope on sinuosity-driven hyporheic exchange flow and**
2 **residence time distribution during a dynamic flood event**

3

4 **Manuscript submitted to Hydrology and Earth System Sciences**

5

6 Yiming Li^{1,2}, Uwe Schneidewind², Zhang Wen^{1*}, Stefan Krause², Hui Liu¹

7

8 ¹Hubei Key Laboratory of Yangtze River Catchment Environmental Aquatic Science,
9 School of Environmental Studies, China University of Geosciences, People's Republic
10 of China

11 ²School of Geography, Earth and Environmental Sciences, University of Birmingham,
12 UK

13

14 ***Correspondence:** Zhang Wen (wenz@cug.edu.cn)

15 **Abstract.** This study uses a reduced-order two-dimensional (2-D) horizontal model to
16 investigate the influence of riverbank slope on the ~~bank storage and~~ sinuosity-driven
17 hyporheic exchange ~~flux (HEF) process~~ along sloping alluvial riverbanks during a
18 transient flood event. The Deformed Geometry Method (DGM) is applied to quantify
19 the displacement of the sediment-water interface (SWI) along the sloping riverbank
20 during river stage fluctuation. This new modeling approach serves as the initial step
21 ~~to focusing on the impact of bank slope on the hyporheic exchange flux (HEF) and the~~
22 ~~residence time distribution (RTD) of pore water in the fluvial aquifer for a sinuosity-~~
23 ~~driven river corridor consider complicated floodplain morphologies in physics-based~~
24 ~~models for better predictions of HEF.~~ Several controlling factors, including sinuosity,
25 alluvial valley slope, ~~and~~ river flow advective forcing and duration of flow are
26 incorporated into the model to investigate the effects of bank slope ~~o~~in aquifers of
27 variable hydraulic transmissivity. Compared to simulations of a vertical riverbank,
28 sloping riverbanks were found to increase the HEF. For sloping riverbanks, the
29 hyporheic zone (HZ) encompasses ~~s~~a larger area and penetrated deeper into the alluvial
30 aquifer, especially in aquifers with smaller transmissivity (i.e., ~~due to larger~~
31 ~~aquifer increased~~ hydraulic conductivity or ~~smaller reduced~~ specific yield). Furthermore,
32 consideration of sloping banks as compared to a vertical river bank can lead to both
33 underestimation or overestimation of the pore water ~~residence time~~ travel time. The
34 impact of bank slope on residence time was more pronounced during a flood event for
35 high transmissivity aquifer conditions, while it had a long-lasting influence after the
36 flood event in lower transmissivity aquifers. Consequently, this decreases the ~~residence~~
37 ~~travel~~ time of ~~HEF water discharging into the river~~ relative to ~~the~~ base flow conditions.
38 These findings highlight the need for (re)consideration of the importance of more
39 complex riverbank morphology as control of hyporheic exchange in ~~alluvial~~
40 ~~aquifers floodplains~~. The results have potential implications for river management and
41 restoration and the management of river and groundwater pollution.

42

43 **Key words:** hyporheic exchange, sloping riverbank, ~~transient river stage~~deformed
44 geometry, ~~peak flow event~~numerical simulation, residence time distribution
45

Nomenclature

ΔL	Nodal spacing [m]
∇	Laplace operator
α_L	Longitudinal dispersivity [L]
α_T	Transverse dispersivity [L]
D	Dispersion-diffusion tensor [L^2T^{-1}]
D_L	Water diffusivity [L^2T^{-1}]
J_x	Base groundwater gradient [-]
K	Hydraulic conductivity [LT^{-1}]
n	Scaling number [-]
n_0	Intensity of flood event [-]
n_d	Skewness of flood event [-]
S_y	Specific yield [-]
t_d	Duration of flood event [T]
t_p	Time to peak river stage [T]
α	Amplitude of the river boundary [L]
Γ_d	Dimensionless aquifer transmissivity [-]
δ	Bank slope angle [$^\circ$]
δ_{ij}	Kronecker delta function [-]
ϵ	Tortuosity [-]
η	Degree of flood event asymmetry [T^{-1}]
θ	Effective porosity [-]
λ	River boundary wave length [L]
σ	River boundary sinuosity [-]
τ	Residence time [T]
ω	Flood event frequency [T^{-1}]
$h(\mathbf{x}, t)$	Transient groundwater head [L]
Δh^*	Dimensionless parameter of ambient groundwater flow [-]

$A^{**}(t)$	Dimensionless variation of HZ area relative to base flow conditions [-]
$C(\mathbf{x}, t)$	Solute concentrations in the aquifer [ML^{-3}]
$C_0(\mathbf{x})$	Solute concentrations as initial condition [ML^{-3}]
$C_S(\mathbf{x}, t)$	Solute concentrations in the river [ML^{-3}]
$d^{**}(t)$	Dimensionless variation of HZ penetration distance relative to base flow conditions [-]
$H(\mathbf{x}, t)$	Thickness of the saturated aquifer [L]
$H_0(\mathbf{x})$	Initial river stage [L]
H_p	Peak river stage during the flood event [L]
$H_r(t)$	River stage at the downstream end [L]
$h_r(x, t)$	Transient river stage [L]
$M(t)$	Displacement of the sediment-water interface [L]
P_e	Péclet number [-]
\mathbf{q}	Specific discharge or Darcy flux [LT^{-1}]
\mathbf{Q}	Aquifer-integrated discharge [L^2T^{-1}]
$Q_{in, HZ}^*(t)$	Dimensionless net flux along the river boundary [-]
$Q_{in, HZ}^*(t)$	Dimensionless exchange flux from the aquifer to the river [-]
$Q_{out, HZ}^*(t)$	Dimensionless exchange flux from the river to the aquifer [-]
$Y(x, t)$	Location of the sediment-water interface boundary [L]
$z_b(\mathbf{x})$	Elevation of the underlying impermeable layer [L]
Γ_d	Dimensionless parameter of aquifer transmissivity [-]
$\mu(\mathbf{x}, 0)$	Mean (first order of) residence time distribution [T]
$\mu_{out}^*(x, t)$	Flux-weighted ratio of mean RT to mean RT under baseflow conditions [-]
$\mu_n(\mathbf{x}, t)$	n -th moment of residence time distribution [T^n]
$\mu_r^*(\mathbf{x}, t)$	Residence time distribution ratio between slope and vertical river bank model [-]
$\mu_{\tau 0-\max}$	Maximum RT in the domain [T]

$\mu_{\tau-s}(\mathbf{x}, t)$	Residence time distribution of slope river bank model [T]
$\mu_{\tau-v}(\mathbf{x}, 0)$	Residence time distribution of vertical river bank model [T]
$\rho(\mathbf{x}, t, \tau)$	Residence time distribution [T]

Abbreviations

HZ	Hyporheic zone
HEF	Hyporheic exchange flux
DGM	Deformed Geometry Method
SWI	Sediment-water interface
RTD	Residence time distribution
RT	Residence time
ALE	Arbitrary Lagrangian–Eulerian
2-D	Two-dimensional
<u>BTS</u>	<u>Biogeochemical timescale</u>

46

47

48 1. Introduction

49 The hyporheic zone (HZ) can be described as the region that connects the river
50 channel and adjacent aquifer, and includes riverbed and riverbanks. Mixing and
51 transporting of different water types (groundwater, surface water) and ages in the HZ
52 driven by hydrodynamic and hydrostatic factors causes spatially and temporally
53 varying exchange of water and biogeochemical species, ~~and energy~~ between river
54 channel, riverbed and aquifer (Cardenas, 2009b; Hester and Gooseff, 2010; Krause et
55 al., 2011, 2017, 2022; McClain et al., 2013; Boano et al., 2014). The hyporheic
56 exchange flux (HEF) represents the interaction flux between surface water and
57 groundwater Hyporheic exchange flow in vertical (e.g., bedform-driven) and horizontal
58 (e.g., meander-driven) ~~domains—directions, which~~ can add to general regional
59 groundwater ex-filtration and infiltration ~~upwelling or downwelling, with HEF~~
60 ~~representing those surface flow components that penetrate and transport through the~~
61 ~~hyporheic sediment and back into the stream.~~ The distribution of hyporheic flow paths
62 strongly determines the spatial and temporal distribution of hydrobiogeochemical
63 characteristics of water within the riverbed and the wider river corridor as well as the
64 formation of so-called hot zones and hot moments (Krause et al., 2013, 2017; Cardenas,
65 2015; Pinay et al., 2015).

66 Hyporheic exchange flux (HEF) is controlled by parameters such as stream
67 discharge dynamics, recharge, riverbed and aquifer hydraulic properties, local ~~pressure~~
68 hydraulic head fluctuations, ~~and as well as~~ river geometry and morphology including
69 sinuosity and riverbank slope (Larkin and Sharp, 1992; Gomez-Velez et al., 2012; 2017;
70 Schmadel et al., 2016). For example, Cardenas et al. (2004) demonstrated how riverbed
71 characteristics and especially the heterogeneity of hydraulic conductivity could
72 increase ~~the hyporheic exchange intensity~~ HEF by 17% to 32%. As such, to be able to
73 better estimate the relative importance of HEF on catchment water fluxes and
74 ~~bio~~ geochemistry geochemical processes ~~requires~~ require a good understanding of ~~the~~ its

75 ~~interactions of its~~ different drivers and controls. This is imperative as the spatiotemporal
76 evolution of HEF ~~paths~~, the resulting change in HZ ~~extent~~ (area) and thus also the ~~mean~~
77 residence ~~or travel~~ time (RT) of the exchanged water in the HZ have significant impact
78 on flow dynamics and transient storage along the river continuum and in turn control
79 ~~the attenuation~~ capacity for contaminant attenuation (Weatherill et al., 2018) and
80 biogeochemical functions of river corridors (Bertrand et al., 2012; Boulton et al., 2010;
81 Brunke and Gonser, 1997).

82 Both lateral exchange between river and its flood-plain, as well as bedform-
83 induced vertical exchange at the streambed interface have been found to be crucial with
84 regards to HEF and the biogeochemical transformation potential along the river corridor
85 (Boano et al., 2010, 2014; Gomez-Velez and Harvey, 2014; Gomez-Velez et al., 2015,
86 2017; Kiel and Cardenas, 2014; Stonedahl et al., 2013). ~~Considerable progress~~
87 of ~~Through using numerical simulations, numerical simulation~~ considerable progress
88 has been made with regards to ~~in~~ our understanding of how river planform geometry
89 (Boano et al., 2006, 2010; Cardenas 2006; 2008; 2009a, 2009b; Stonedahl 2013),
90 dynamic flood events (Gomez-Velez et al., 2012; 2017) and evapotranspiration
91 (Kruegler et al., 2020) control HEF. Focusing on lateral exchange flow processes,
92 Cardenas (2008; 2009a, 2009b) ~~developed~~ utilized numerical models to investigate
93 HEF and residence time distribution (RTD) for various river channel morphologies and
94 regional groundwater flow conditions. Their simulations indicate that channel
95 morphology, represented by sinuosity, is a dominant factor controlling HEF, the total
96 HZ area, and RTD. In addition, Boano et al. (2010) used a similar modeling framework
97 to study the relationship between RTD and biogeochemical transformation by
98 introducing surface water as a major source of dissolved organic matter that triggers a
99 sequence of redox reactions within the HZ. Reactive transport simulations showed a
100 good relationship between RTD and denitrification reaction potential. Based on these
101 studies, Gomez-Velez et al. (2012) conducted numerical simulations to investigate the
102 impact of aquifer parameters (water table gradient, hydraulic conductivity, dispersivity)

103 and channel sinuosity on HEF and RTD. By comparing RTD with the timescale of
104 ~~nitrate-forming nitrification/denitrification reactions or reducing reactions~~, a meander
105 can be classified as a source or sink of nitrate ~~for (de)nitrification activities~~. More recent
106 modeling studies ~~have~~—focused predominantly on the effects of dynamic
107 river/groundwater stage fluctuations on lateral (e.g., Schmadel et al., 2016; Gomez-
108 Velez et al., 2017) and vertical (e.g., Singh et al., 2019, 2020; Wu et al., 2018, 2020,
109 2021) hyporheic exchange and RTD. For example, Gomez-Velez et al. (2017) explored
110 the HZ response to a dynamic river stage ~~under due to different parameter values~~
111 ~~for variable~~ hydraulic conductivity, ~~river stage during flood events~~, groundwater ~~flow~~
112 gradient and river sinuosity conditions. Their results indicate that the dynamic forcing
113 greatly influences net HEF, the area of HZ and RTD across different scenarios, whereby
114 higher aquifer transmissivity will likely result in a stronger but shorter response of HEF
115 and RTD to a flood event.

116 Although there is a considerable body of numerical research on the lateral
117 hyporheic response to the various geometrical (e.g., geometry of river channel, river
118 slope, etc) and dynamic drivers (e.g., fluctuation of river/groundwater, gaining and
119 losing conditions of groundwater, etc), many HZ studies do not specifically consider
120 floodplain-driven processes or they apply vertical riverbanks with straight river
121 planimetry in an attempt to reduce model complexity in line with the analytical or
122 numerical solutions used (Cooper and Rorabaugh, 1963; Hunt, 1990; Schmadel et al.,
123 2016; Gomez-Velez et al., 2017;). However, riverbanks are usually ~~tilted sloping~~
124 ~~(inclined)~~—rather than vertical (Liang et al., 2018) as they undergo erosion (Osma and
125 Thorne, 1988). Previous research has proven that bank erosion and bank collapse are
126 globally spreading processes controlled by various factors, such as initial bank slope
127 angle (Zingg, 1940; Lindow et al., 2009), surface flow forces (Hagerty et al., 1995; Fox
128 and Wilson, 2010), vegetation cover (Mayor et al., 2008; Gao et al., 2009; Puttock et
129 al., 2013) and sediment properties (Millar and Quich, 1993). Neglecting bank slope in
130 analytical and numerical model solutions may therefore have a significant influence on

131 the prediction accuracy of HEF (Doble et al. 2012a, 2012b) and RTD (Dex et al., 2014;
132 Siergieiev et al., 2015) in an unconfined floodplain aquifer. Thus, a detailed analysis of
133 the floodplain drivers of HEF should require a more detailed consideration of the
134 floodplain geometry including riverbank slope in bank storage conceptual models
135 (Sharp, 1977).

136 A few previous studies have used numerical modeling where the model is
137 bounded by a sloping riverbank to assess the influence of bank slope on HEF for a
138 vertical section of an alluvial aquifer. In such cases, the aquifer was considered variably
139 saturated, homogenous, and isotropic, while flow in the unsaturated zone was
140 calculated using the Richards equation (Li et al., 2008; McCallum et al., 2010; Doble
141 2012a; b). These studies have confirmed that neglecting bank slope can lead to an
142 underestimation of the bank storage volume as well as the temporal HEF in vertical
143 cross-sectional profiles, especially under relatively small bank angles.

144 In turn, river sinuosity and ambient groundwater gradient (along the river
145 channel) have not been studied as potential drivers of sinuosity-driven lateral HEF and
146 RTD and their biogeochemical implications ~~under complex riverbank morphological~~
147 ~~conditions~~ when a sloping river bank exists and it needs to be determined whether
148 considering both drivers can lead to significantly different findings as compared to
149 previous cross-sectional profile models (Doble et al., 2012; Siergieiev et al., 2015; Dex
150 et al., 2014). In this study, we therefore quantify the effect of bank slope on the
151 ~~simulated~~ spatial extent (area) of the HZ in sinuosity-driven river meanders and how it
152 impacts the evolution of HEF and RTD under varying aquifer transmissivity conditions
153 to better understand lateral HEF through the alluvial plain. We build on the conventional
154 numerical modeling approach introduced by Gomez-Velez et al. (2017) and consider
155 lateral bank slope by ~~using a deformed geometry method (DGM) approach. For this,~~
156 ~~we couple~~ the deformed geometry method (DGM) with the Boussinesq
157 equation ~~into the flow (Liang et al. 2020), the vertically integrated solute transport~~
158 ~~equation~~ and the residence time distribution equation ~~to study HEF~~. Our results reveal

159 how and when bank slope plays an important roles in predicting HEF will help to reveal
160 the importance of bank slope for the prediction of HEF and RTD in sinuosity-driven
161 meandering rivers with respect to HEF and RTD-, which in turn will lead to an improved
162 understanding of the river channel-aquifer-floodplain system and provide guidance on
163 the placement of monitoring locations in river management studies. for the
164 conceptualization hypothesis of numerical model and the monitoring location selection
165 of field study in the future.

166

167 2. Methodology

168 2.1 Model setup ~~with~~ using deformed geometry method

169 ~~Our modeling approach builds on the work of~~ The conventional model modeling
170 approach and dimensionless parameterization metrics used in by Gomez-Velez et al.
171 (2017), ~~who developed a comprehensive simulation tool in dimensionless form that~~ can
172 represent most riverbank-aquifer situations and dynamic flood conditions. In our study,
173 we use their conceptual model to set up a baseline case ~~as a baseline~~ with the same
174 model frame, equations and parameterization metrics. Additional information regarding
175 the implementation of this baseline ~~model case~~ can be found in the SI ~~as S1 to S3 and~~
176 ~~Gomez-Velez et al. (2017)~~. However, where their previous research assumed a vertical
177 river bank for sinuosity-driven HEF models ~~where Gomez-Velez et al. (2017) assume a~~
178 ~~vertical riverbank~~, we consider a sloping riverbank and use the DGM approach to
179 capture the dynamic evolution of the SWI along the river course. A constant sloping
180 angle (δ [°]) along the alluvial riverbank of a sinusoidal river was implemented in our
181 model (see blue lines of conceptual model in Figure S1 and the corresponding
182 mathematical model in Figure S2a) while the surface water interface (SWI) was
183 assumed to be always vertical (vertical solid red and green lines in Figure S2c). As such,
184 the contraction or expansion of the simulated domain, i.e., displacement of the SWI can
185 be characterized by the sloping angle (there is no movement of the SWI for the vertical
186 riverbank case) and river stage. As the river stage changes, so does the location of the
187 SWI.

188 When the river stage changes in our model, the sinusoidal boundary will migrate
189 towards or away from the floodplain meaning that the submerged part of the riverbank
190 is considered contracted and our model only considers the alluvial aquifer that is not
191 submerged. The evolution of the SWI during a flood event can be calculated by

192 considering river stage and bank slope via:

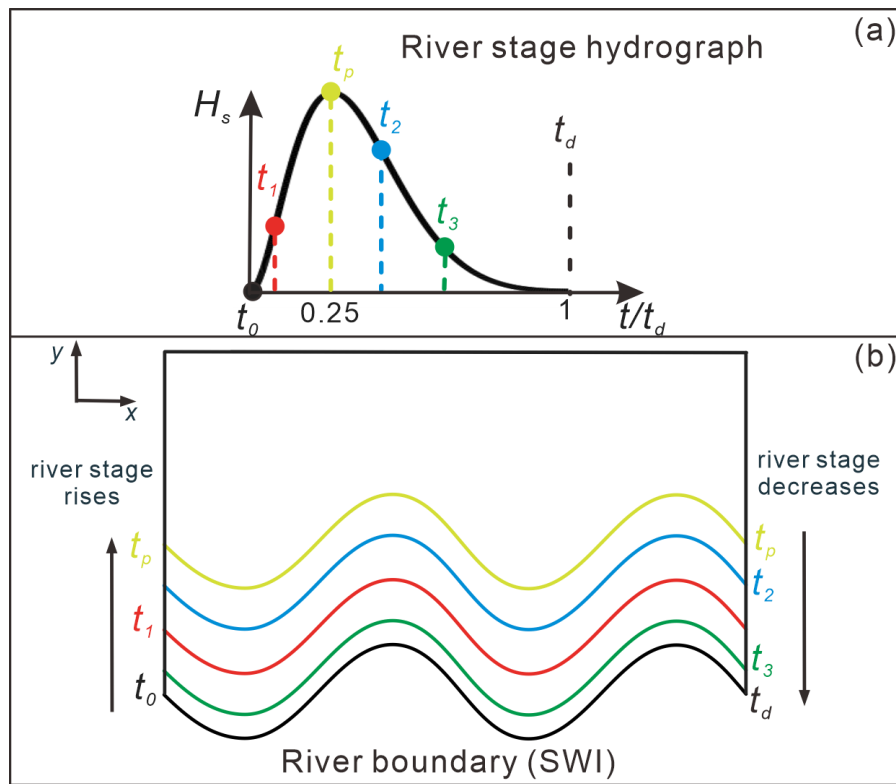
$$193 \quad Y(x, t) = Y_0(x) + M(t) \quad (1)$$

194 where $Y(x, t)$ [L] is the location of the SWI boundary while; $Y_0(x)$ [L] is the initial
195 location of the SWI. In contrast to Gomez-Velez et al. (2017), the displacement of the
196 SWI caused by the deformation of the model domain ($M(t) = [h(t) - h(0)]/\tan(\delta)$, where
197 $h(t)$ [L] is transient hydraulic head) is added in Eq. (1), which represents the
198 displacement of the river boundary in y -direction due to river stage fluctuation and bank
199 slope angle (see the horizontal distance between the vertical red and green solid line in
200 Figure S2c).

201 To simulate the model domain deformation and mesh displacement, we use the
202 DGM interface in COMSOL. In this interface, the deforming feature of a specified
203 domain can be defined as a boundary condition with a given moving velocity or
204 displacement. DGM is based on the arbitrary Lagrangian–Eulerian (ALE) method,
205 which is a hybrid method that allows both the model domain and mesh to move or
206 deform simultaneously in a predefined manner. More details on ALE can be found in
207 Donea et al. (2014). While it has previously been used for simulating general free-
208 surface problems (e.g., Duarte et al., 2004; Maury, 1996; Pohjoranta and Tenno, 2011),
209 to our knowledge, DGM has not yet been implemented to solve moving boundary
210 problems in hyporheic exchange studies. Here we used Eq. (1) as an input to the DGM
211 interface to simulate the displacement of the SWI (water flow) during a dynamic flood
212 event. Infiltration and seepage face before and after the peak time of the flood event,
213 respectively, were neglected (Boano et al., 2006; Cardenas. 2009a, b; Kruegler et al.,
214 2020). Fig. 1 illustrates the river stage hydrograph of this study (Fig. 1a, calculated by
215 Eq. (S2)) and the diagram of the displacement of the SWI (Fig. 1b) during the flood
216 event after coupling DMGGM into the model. The colored river boundaries in Fig. 1b
217 are corresponding to the times of colored dots in Fig. 1a. Additionally, solute transport
218 and RTD were simulated based on the extent of the flow field according to Gomez-
219 Velez et al. (2017), as shown in the SI as-(S2 and S3, respectively).

220

221



222

223 **Figure 1.** (a) River stage hydrograph during the flood event; (b) diagram showing of
 224 displacement of SWI (Fig. 1b) during the flood event. The colored SWIs in Fig. 1b(b)
 225 are corresponding to the times of colored dots in Fig. 1a(a). The When the river stage
 226 increases, the river boundary migrates into the aquifer during the raising of
 227 river stage, and recovers to its initial location as river stage decreases. The upward
 228 and downward arrow in Fig. 1b indicates the raising and decreasing of river stage,
 229 respectively.

230

231 Additionally, solute transport and RTD were simulated based on the extent of the
 232 flow field according to Gomez-Velez et al. (2017), as shown in the SI.

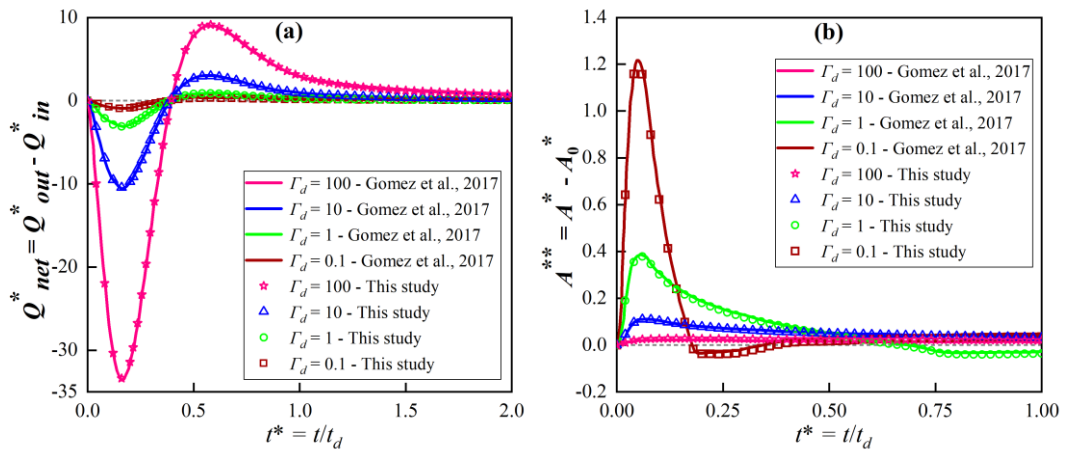
233 2.2 Model parameterization, testing and scenarios

234 Model h Hydraulic conditions used in our numerical modeling study are based on

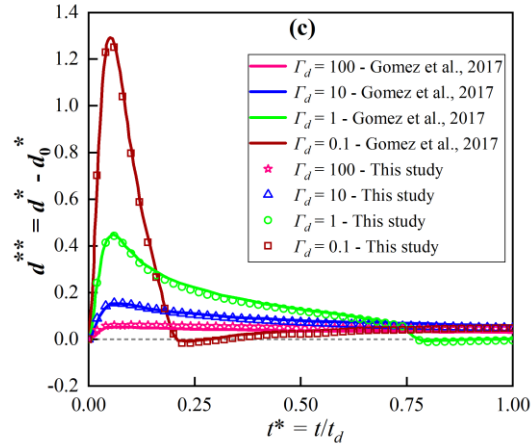
235 values from Gomez-Velez et al. (2017), who conducted a Monte Carlo analysis. They
 236 found that the dynamic variations of HEF and RTD are mainly determined by ambient
 237 groundwater flow w (referred to as dimensionless parameter $\Delta h^* = \frac{J_{st}^2}{0.5(1+n_0)H_0}$, see Table
 238 1) and the ratio of aquifer hydraulic conductivity to the duration of the flood event
 239 (referred to as dimensionless constant $\Gamma_d = \frac{S_y \lambda^2}{0.5K(1+n_0)H_0 t_d}$, see Table 1 and Fig. S2, where
 240 S_y is specific yield [-]; λ is wave length of sinuous river; K is hydraulic conductivity
 241 [LT^{-1}]; n_0 is intensity of flood event [-] H_0 is base river stage [L]; t_d is duration of flood
 242 event [T]).

243 After setting up the ~~original model of Gomez-Velez et al. (2017) as a~~ baseline
 244 model case with a vertical riverbank ($\delta = 90^\circ$), we compared our model results for that
 245 case with those obtained by Gomez-Velez et al. (2017) for (a) net HEF represented by
 246 $Q_{net, HZ}^*(t)$; (b) area of HZ, $A^{**}(t)$; (c) penetration of the HZ, $d^*(t)$ for $\Gamma_d = 0.1, 1, 10$
 247 and 100, and found that our model simulated those cases with high accuracy (Fig. 2+).
 248 Parameters $A^{**}(t)$ and $d^*(t)$ are based on modeling the transport of a conservative solute
 249 while $Q_{net, HZ}^*(t)$ is based on modeling water flow. Slight differences between our model
 250 and that of Gomez-Velez et al. (2017) might be due to the use of a much more refined
 251 mesh in this study as well as ~~and~~ different length scales.

252



253



254
 255 **Figure 21.** Comparison of results obtained in this study with those of Gomez et al.
 256 (2017) for the baseline case with a vertical river bank and variable Γ_d : (a) net hyporheic
 257 exchange flux represented by $Q_{net, HZ}^*(t)$; (b) extent of the hyporheic zone $A^{**}(t)$ and (c)
 258 penetration distance $d^*(t)$ of the hyporheic zone into the alluvial valley. A more refined
 259 mesh and different length scales used in this study, can explain ~~occasional~~ slight
 260 ~~differences~~ variations between our model and that of Gomez et al. (2017) ~~might occur~~.
 261 Information regarding model fits can be found in the SI.

262 To test, whether our assumption

263 Furthermore, the appropriateness of the assumption of considering a vertical SWI
 264 and the implementation of using DM the DGM to characterize the migration of the SWI
 265 was validated appropriate, we ~~by comparing~~ the vertical 2-D model and the
 266 1-D model coupled with DMG the DGM. Detailed information for the
 267 implementation on this comparison as well as of validation models and the validation
 268 results are listed in the SI in section as S4. The results show that the our assumptions
 269 vertical SWI and using of DMG approach is ~~reasonable of this study are appropriate~~
 270 for when simulating HEF in a sloping river-bank aquifer.

271 We then considered a series of riverbank scenarios where the bank slope angle
 272 ranged from $\delta = 90^\circ$ (vertical riverbank) to 10° (nearly horizontal case) and Γ_d values
 273 ranged from 0.1 to 100, (corresponding to aquifer hydraulic conductivity ranging from
 274 480 to 0.048 m/d, indicating high to low transmissivity. Table 1 presents the parameters
 275 used in our numerical modeling study. The finite-element models proposed in this study

276 were [developed set up](#) using the COMSOL Multiphysics (COMSOL) software. Eq. (S1),
 277 Eq. (S3) and Eq. (S6) were implemented by [using customizing a Partial Differential](#)
 278 [Equation](#) (PDE) interface to include the Boussinesq [equation](#), vertical integrated solute
 279 transport [equation](#) and [RTD—equation for calculating residence \(travel\) time](#)
 280 [distributions \(RTD\)](#), respectively. The model domain was discretized into about 0.5
 281 million variably-sized triangular elements, with refinement imposed near the river
 282 boundary. Mesh-independent numerical solutions are achieved by limiting grid size (ΔL)
 283 to less than 0.2 m. Thus, the transverse and longitudinal Peclet numbers (calculated by
 284 $P_e = \Delta L / \alpha_L$ and $P_e = \Delta L / \alpha_T$, respectively) in both advection and diffusion dominated
 285 zones are less than 1, which is smaller than the upper limit of $P_e = 4$ to effectively avoid
 286 numerical oscillations and instabilities.

287

288 **Table 1.** Parameters and values used in our numerical model simulations. [\(adopted from](#)
 289 [Gomez Velez et al. \(2017\)\)](#).

Parameters	Value	Description
Constant model parameters		
S_y	0.3	Specific yield [-]
λ	40	River boundary wave length [L]
α	5	River boundary amplitude [L]
θ	0.3	Efficient porosity [-]
J_x	0.0025	Base groundwater gradient [-]
σ	1.14	River boundary sinuosity [-]
t_d	10	Duration of flood event [T]
n_d	0.25	Skewness of flood event [-]
t_p	$n_d t_d$	Time to peak river stage [T]
H_0	1	Base river stage [L]
n_0	1	Intensity of flood event [-]
α_L	2	Longitudinal dispersivity [L]

α_T	$0.1 \alpha_L$	Transverse dispersivity [L]
Variable model parameters		
Γ_d	0.1 1 10 100	Dimensionless aquifer transmissivity [-]
δ	90 70 50 20 10	Bank slope angle [°]

290

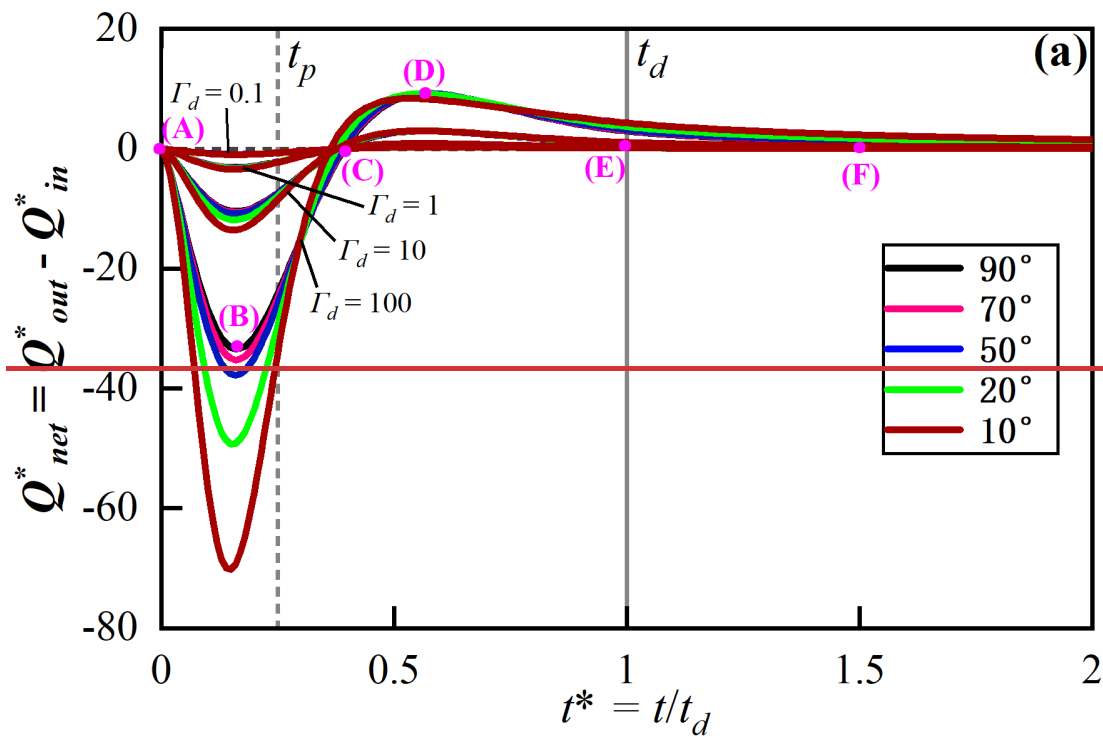
291 Similar to Gomez-Velez et al. (2017), we evaluate the impact of bank slope by
 292 comparing the net hyporheic exchange flux ($Q_{net, HZ}^*(t)$), area of HZ ($A^{**}(t)$),
 293 penetration distance of the HZ ($d^{**}(t)$) and RTD ($\mu_r^*(\mathbf{x}, t)$) between vertical and sloping
 294 river bank models. A detailed definition of these comparison variables are
 295 listed is provided in the SI (section as-S5).

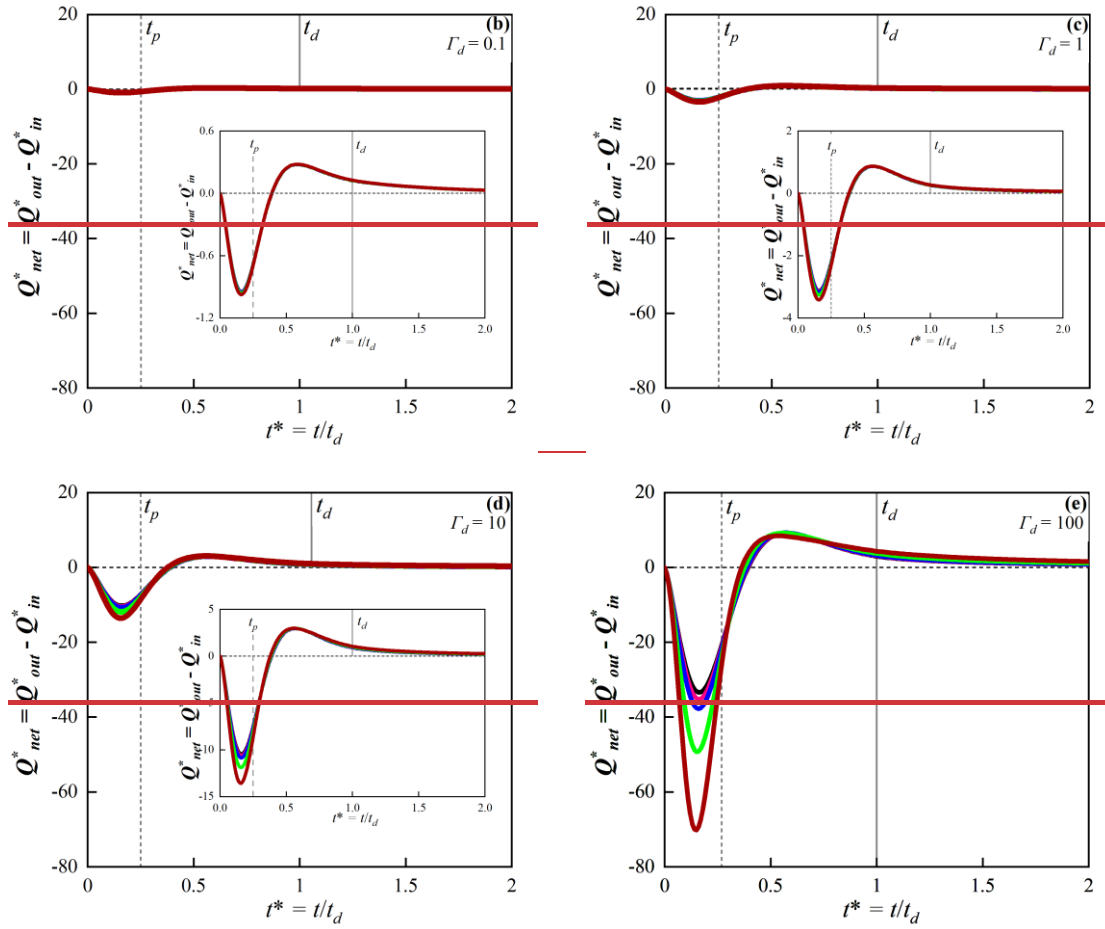
296

297 **3. Results**298 **3.1 Effect of bank slope on hyporheic exchange flow and HZ patterns extent**299 **3.1.1 Hyporheic exchange flow**

300 — The flow field (velocity magnitude and direction) and net HEF ($Q_{net, HZ}^*(t)$)
 301 changed dynamically during and after the simulated flood event. Fig. 2a shows a
 302 comparison of $Q_{net, HZ}^*(t)$ values for different values of δ and F_d . In order to illustrate
 303 the influence of δ on $Q_{net, HZ}^*(t)$ under different F_d conditions more clearly, Fig. 2b–2e
 304 highlight the $Q_{net, HZ}^*(t)$ evolution for a given F_d at smaller scale. Snapshots of the flow
 305 field and the boundary of the HZ area (isolines of $C(x, t) = 0.5$ as concentration of a
 306 conservative solute) for different δ conditions at different times (pink dots in Fig. 2a)
 307 for $F_d = 1$ are shown in Fig. 3a–3f.

308





310

311

312

313

314

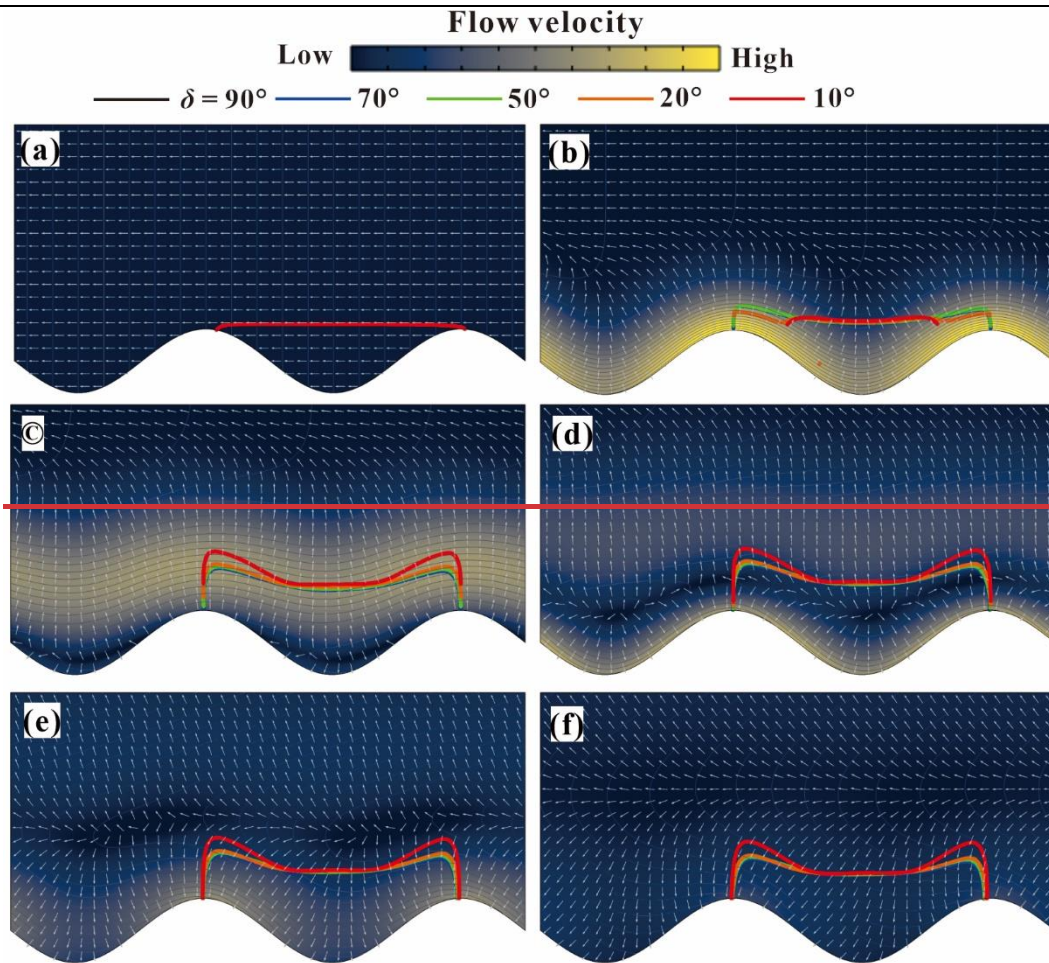
315

316

317

318

Figure 2. (a) Temporal evolution of dimensionless net flux for alternative values of F_d and δ (colored lines). The results for each F_d condition from 0.1 to 100 and different slopes are shown again in Fig. 2b–2e separately, to represent smaller scales. In each figure, time to peak (t_p) and flood duration (t_d) are marked by vertical dashed lines. Pink dots in (a) marked by (A)–(F) correspond to the snapshots of the flow field shown in Fig. 3. A negative flux value here represents water flow from river to aquifer.



319

320

321

322

323

324

325

326

327

328

329

330

331

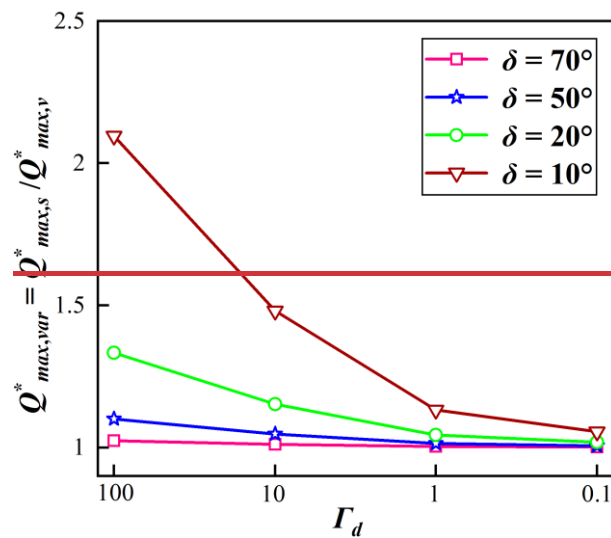
332

Figure 3. Temporal evolution of the alluvial flow field and spatial extent of the HZ. Snapshots of the flow field at different time steps during the simulated event (pink dots in Fig. 2a). Colored surfaces represent the magnitude of the Darcy flux vector (blue is low and yellow is high) and white isolines the dimensionless hydraulic head. Bold colored lines correspond to the HZ extent for different bank slope conditions.

Before the flood event ($t=0$), steady state base flow conditions are assumed, as shown in Fig. 3a. The inflow and outflow (along the upstream and downstream meander bend, respectively) are in balance. The HZ boundaries for different δ conditions in Fig. 3a are the same before the flood event because the bank slope has no influence on the flow field and HZ extent. The onset of the flood event is indicated by the rising river stage and forces the river to infiltrate into the aquifer along the SWI (negative values of $Q_{net, HZ}^*(t)$ in Fig. 2), resulting in the expanded HZ as shown in Fig. 3b. The influx

333 of river water into the HZ ($Q_{net, HZ}^*(t)$) reaches its maximum before the time to peak
 334 river stage ($t = 0.25t_d$) because the pressure wave propagates into the aquifer and
 335 decreases the head gradient between the river and the connected aquifer. An aquifer
 336 with larger F_d limits the propagation of the pressure wave due to the low transmissivity,
 337 which leads to a larger head gradient near the SWI. This, consequently, leads to larger
 338 dimensionless net fluxes under increasing F_d conditions.

339 The maximum dimensionless flux ratios $Q_{max, var}^* = Q_{max, s}^* / Q_{max, v}^*$ of sloping ($\delta < 90^\circ$,
 340 $Q_{max, s}^*$) and vertical ($\delta = 90^\circ$, $Q_{max, v}^*$) riverbank cases are shown in Fig. 4. The bank
 341 slope is found to increase the infiltration flux by up to 120% ($Q_{max, var}^* \sim 2.2$) for $F_d =$
 342 100 with $\delta = 10^\circ$ while for larger slope angles or smaller F_d the dimensionless
 343 infiltration flux gradually decreases. This is because aquifers with smaller F_d (higher
 344 hydraulic transmissivity) are more sensitive to river stage variation and have a strong
 345 ability to transmit the pressure wave into the aquifer. In such cases, the influence of δ
 346 on the net flux becomes less important. On the other hand, a smaller δ induces a longer
 347 displacement of the SWI ($M(t)$) away from the river, where the groundwater head
 348 adjacent to the SWI is always relatively low (i.e., the head in base flow condition).—



351
 352 **Figure 4.** Ratio of maximum negative net flux of slope to no-slope (vertical river bank)

353 conditions $Q_{max,var}^* = Q_{max,s}^* / Q_{max}^*$, and aquifer transmissivities. The ratios of alternative
 354 slope condition are marked by different symbols and colors.

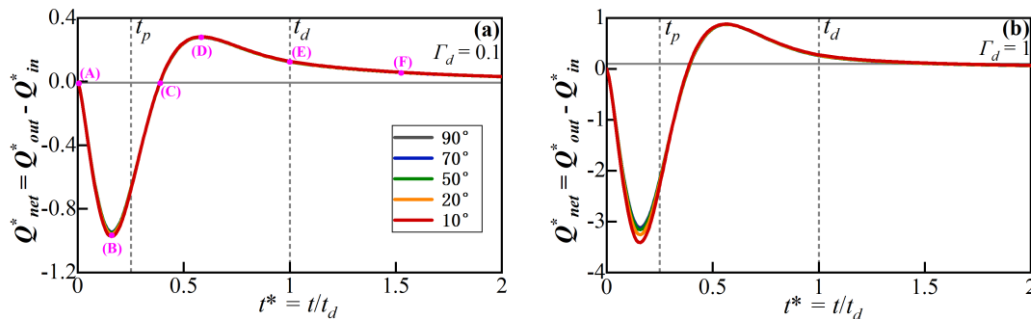
355

356 As the river stage decreases after t_p , the head gradient near the SWI gradually
 357 reverses and the net outflux starts increasing (the river is gaining water). This is
 358 associated with the river stage declining below the groundwater level (see Fig. 3c–3f).
 359 Fig. 2 shows that the bank slope has little impact on the net outflux. Where $F_d = 100$,
 360 bank slope can slightly extend the time required for the system to recover to initial
 361 condition after t_p but in general, the response of the net outflux to bank slope is
 362 negligible when compared to that of the influx. Eventually, the net flux converges to
 363 zero, which indicates the flow field within the aquifer recovers to the initial conditions.

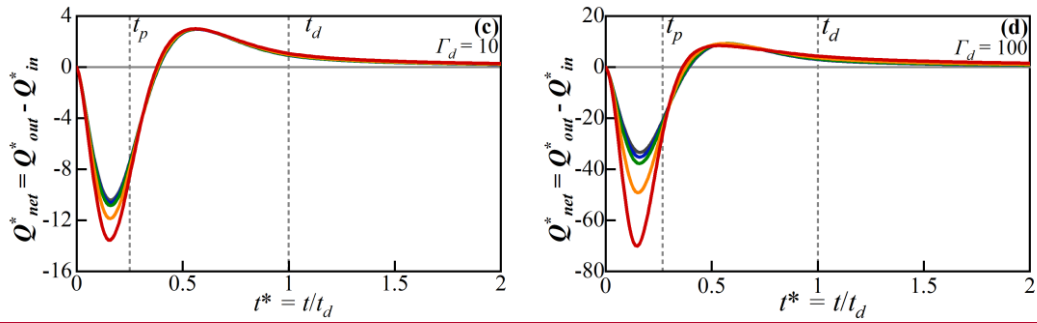
364 3.1.1 Hyporheic exchange flow

365 The flow field (velocity magnitude and direction) and net HEF ($Q_{net, HZ}^*(t)$)
 366 changed dynamically during and after the simulated flood event. Fig. 3a – 3d shows the
 367 evolution of net HEF for different aquifer transmissivity (Γ_d) and bank slope angle (δ)
 368 condition. Snapshots of the flow field and the boundary of the HZ area (isolines of $C(\mathbf{x},$
 369 $t) = 0.5$ as concentration of a conservative solute) for different δ conditions at different
 370 times (pink dots in Fig. 3a) for $\Gamma_d = 1$ are shown in Fig. 4a - 4f.

371



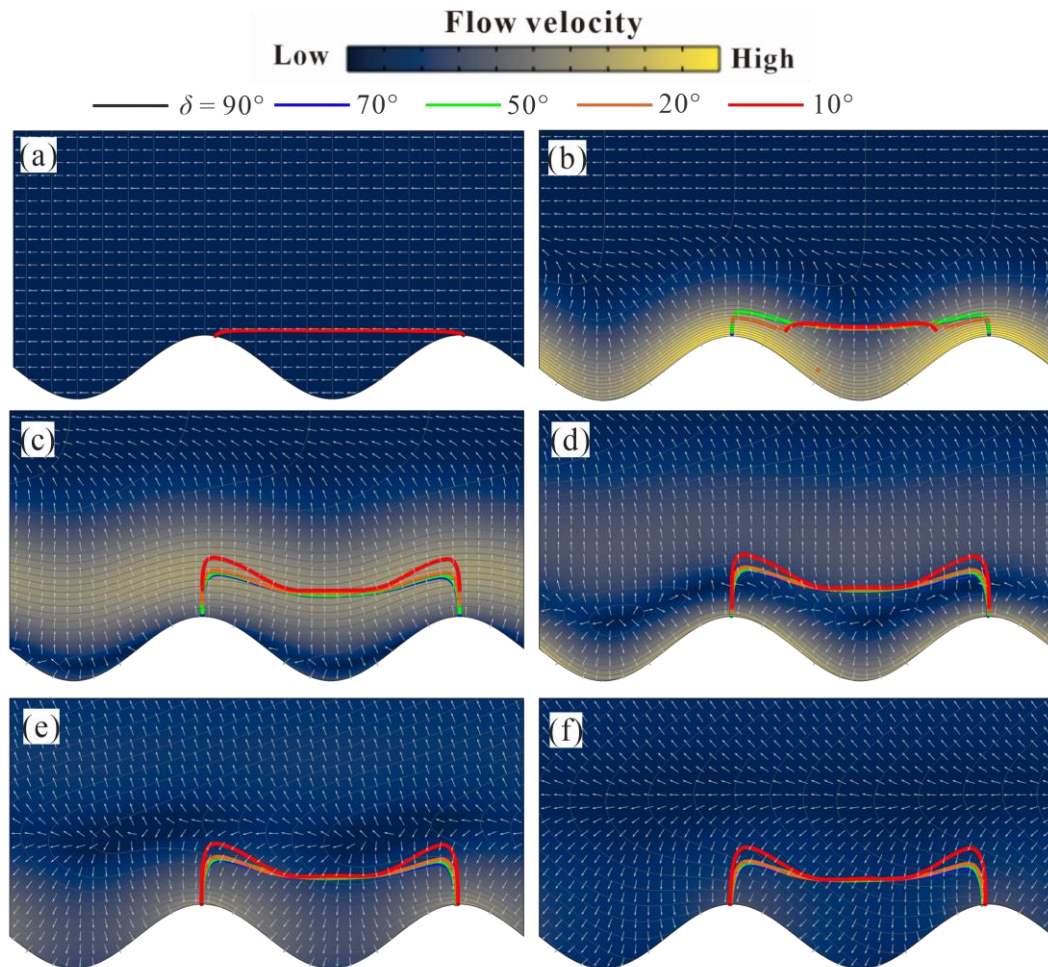
372



373

374 **Figure 3.** Temporal evolution of dimensionless net flux HEF ($Q_{net, HZ}^*(t)$) for four
 375 different aquifer transmissivity values (represented by Γ_d) and bank slopes
 376 condition angles (δ , from 10-90 degrees). Time-to-peak flood (t_p) and flood duration (t_d)
 377 are marked by vertical dashed lines. Pink dots in (a) marked by (A) - (F) correspond to
 378 the snapshots of the flow field shown in Fig. 4. A negative flux value here represents
 379 water flow from river to aquifer. Note that Γ_d negatively correlates with the
 380 transmissivity of aquifer.

381



382

383 **Figure 4.** Plain view of the river channel and aquifer showing of the temporal evolution
 384 of the alluvial flow field and spatial extent of the HZ. (a)-(e) are snapshots of the flow
 385 field at different time steps during the simulated event (pink dots in Fig. 3a). Colored
 386 surfaces represent the magnitude of the Darcy flux vector (blue is low and yellow is
 387 high) and white isolines the dimensionless hydraulic head. Bold colored lines
 388 correspond to the HZ extent for different bank slope conditions. ~~The blue lines for $\delta =$~~
 389 ~~70° were covered due to the small difference compared with other δ conditions.~~

390

391 Before the flood event ($t = 0$), steady-state base flow conditions are assumed, as
 392 shown in Fig. 4a. The inflow and outflow (along the upstream and downstream meander
 393 bend, respectively) are in balance. The bank slope has no effect on the HZ boundaries
 394 before the flood event.

395 Before the peak river stage of the flood event is reached ($0 < t < 0.25t_d$), the onset
 396 of the flood event is indicated by the rising river stage and forces the river to infiltrate
 397 into the aquifer along the SWI (negative values of $Q_{net, HZ}^*(t)$ in Fig. 3), resulting in the
 398 expansion of the HZ as shown in Fig. 4b. The influx of river water into the
 399 HZ ($-Q_{net, HZ}^*(t)$) reaches its maximum before the time-to-peak river stage ($t = 0.25t_d$)
 400 because the pressure wave propagates into the aquifer and decreases the head gradient
 401 between the river and the connected aquifer. For higher transmissivity aquifers (Lower
 402 Γ_d values in Fig. 3), bank slope plays a minor impact on the
 403 calculation of net outflow flux as the fast propagation of the pressure wave results in
 404 the hydraulic head near the SWI to be very similar. Among different aquifer
 405 transmissivity conditions. As aquifer transmissivity decreases, the ability of the aquifer to transmit the pressure wave
 406 becomes limited, while the interaction flux is dominated by the location (displacement) of the
 407 SWI and the river stage. On the other hand, a smaller slope angle induces a longer
 408 displacement of the SWI ($M(t)$) away from the river, where the groundwater head
 409 adjacent to the SWI is always relatively high (i.e., the head in base flow condition).
 410 This, consequently, leads to a larger head gradient near the SWI as well as larger
 411 dimensionless net fluxes under increasing Γ_d conditions as shown in Fig. 3.

414 The maximum dimensionless flux ratios $Q_{max, var}^* = Q_{max, s}^* / Q_{max, v}^*$ of sloping (δ
 415 $< 90^\circ$, $Q_{max, s}^*$) vs vertical ($\delta = 90^\circ$, $Q_{max, v}^*$) riverbank cases are shown in Fig. 5,
 416 which indicates the deviation in predicting peak net flux when neglecting the slope of
 417 the river-bank. The bank slope is found to increase the infiltration flux by up
 418 to 120% ($Q_{max, var}^* \approx 2.2$) for $\Gamma_d = 100$ with $\delta = 10^\circ$ while for larger slope angles or
 419 higher hydraulic transmissivities the dimensionless infiltration flux gradually decreases.

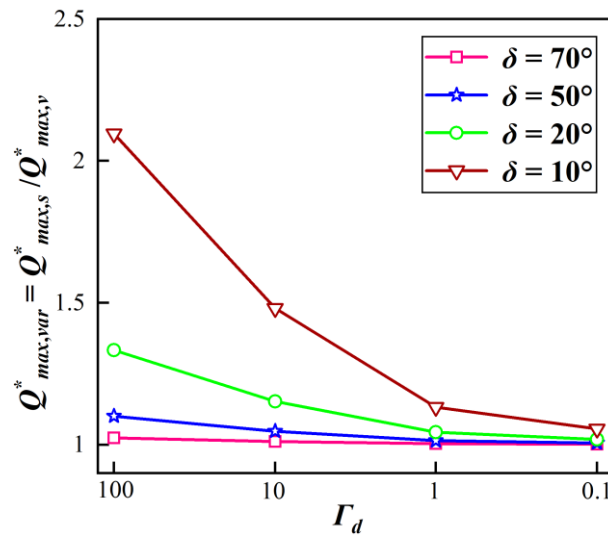


Figure 5. Ratio of maximum negative net flux for slope to no-slope (vertical river bank) conditions $Q^*_{max,var} = Q^*_{max,s}/Q^*_{max,v}$ for various four aquifer transmissivities and slope angles. The ratios of alternative slope condition are marked by different symbols and colors. Note that Γ_d negatively correlation es with the aquifer transmissivity of aquifer.

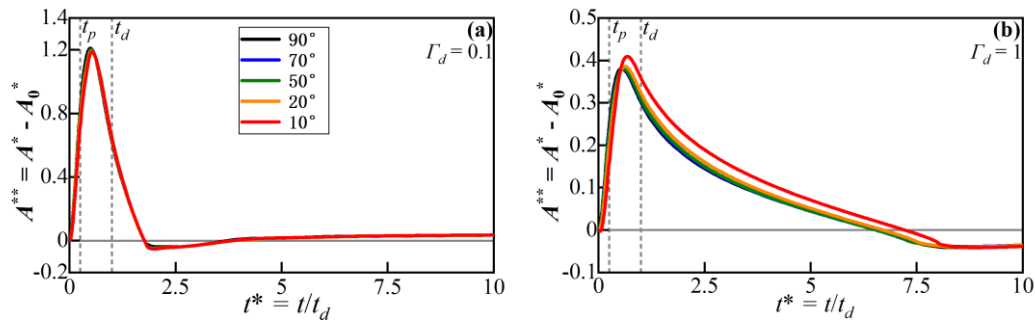
As the river stage decreases after t_p , the head gradient near the SWI gradually reverses and the net outflux starts increasing (the river is gaining water) as shown in Fig. 3. This is associated with the river stage declining below the groundwater level (see Fig. 4c - 4f). The groundwater stage near SWI were similar among different bank slope angle condition after the peak time of flood event, thus, Fig. 3 shows that the bank slope has little impact on the net outflux. For the lowest hydraulic transmissivity condition ($\Gamma_d = 100$), bank slope can slightly extend the time required for the system to recover to initial conditions after t_p but in general, the response of the net outflux to bank slope is negligible when compared to that of the influx. Eventually, the net flux converges to zero, which indicates the flow field within the aquifer recovers to the initial conditions. The bank slope has no impact on the HEF after the duration of flood event.

3.1.2 Patterns of hyporheic area and penetration distance

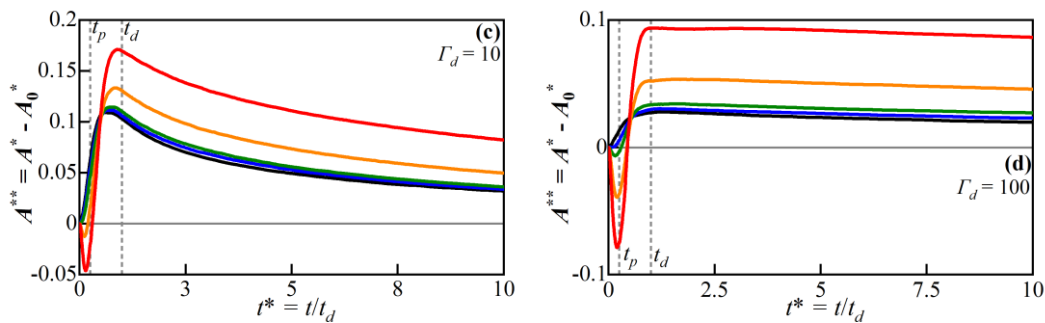
Fig. 65a and Fig. 76a show the temporal evolution of the dimensionless HZ area ($A^{**}(t)$) and penetration distance ($d^{**}(t)$) into the alluvial valley relative to the initial condition for varying aquifer transmissivity (Γ_d) F_d and slope angles, while Fig. 5b—5e and Fig. 6b—6e illustrate the impact of δ on $A^{**}(t)$ and $d^{**}(t)$ for different values of F_d in a close-up. The vertical dash lines in the subfigures of Fig. 6 and Fig. 7 are the time to peak (t_p) and flood duration (t_d)

448

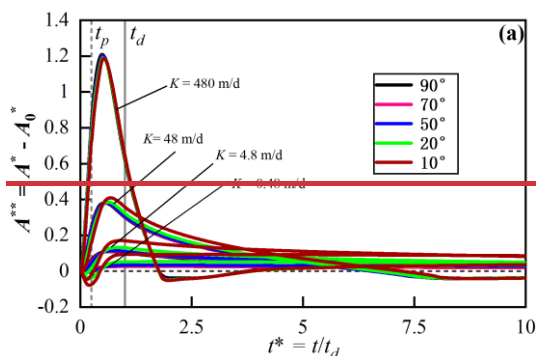
449

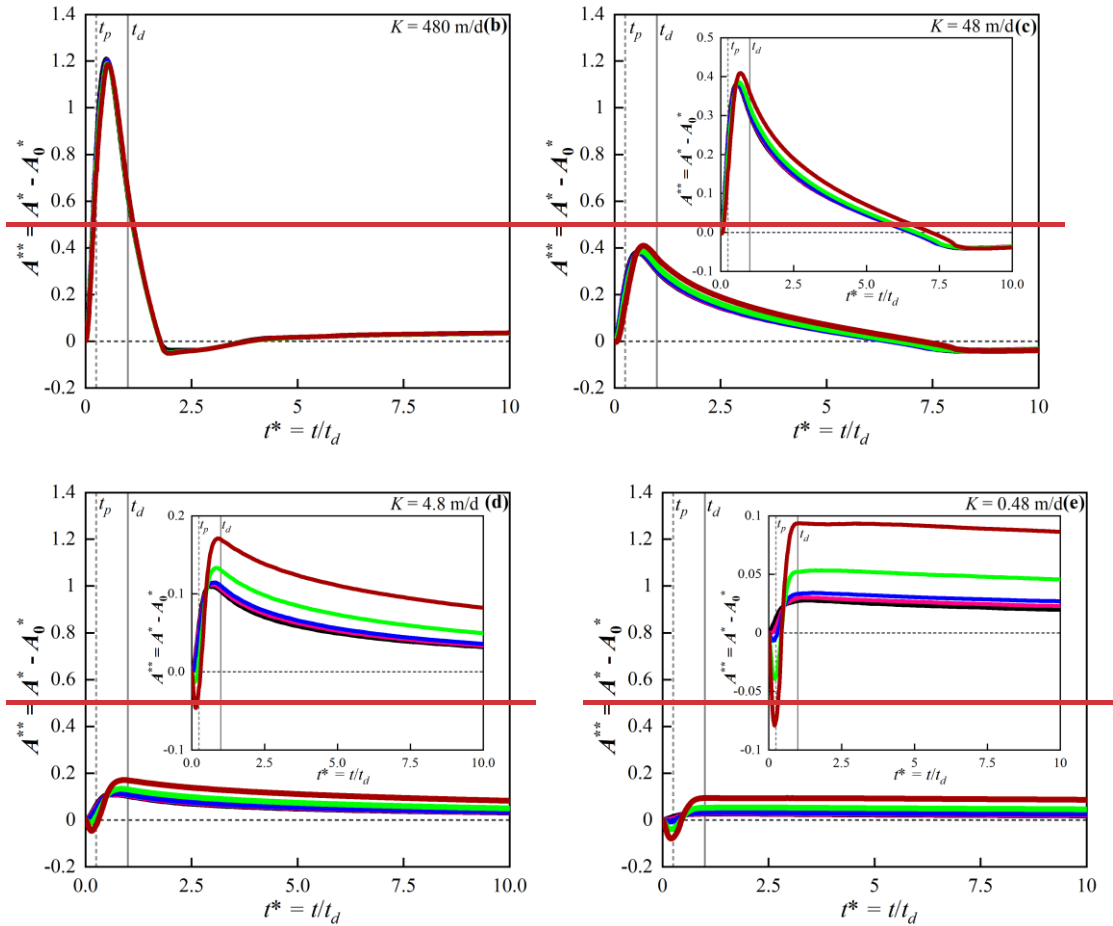


450



451



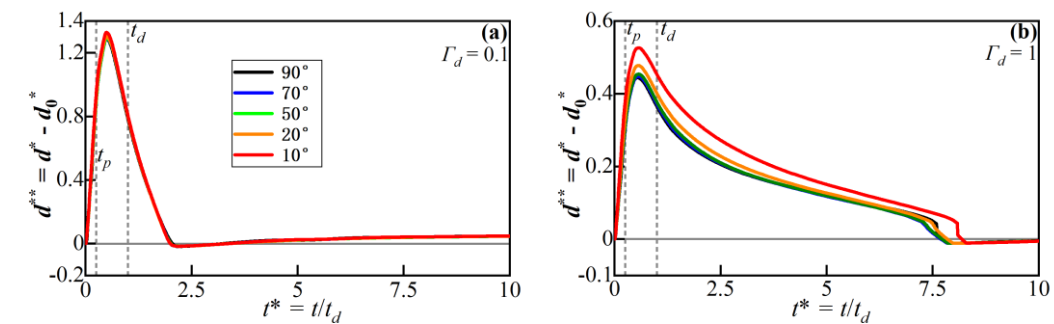


452

453

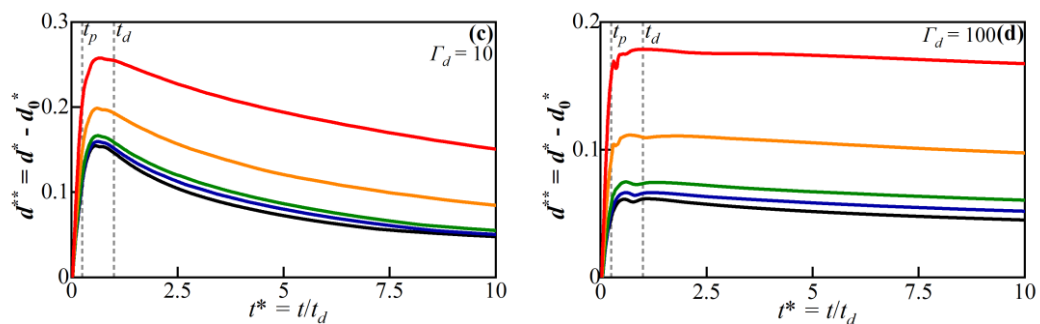
454 **Figure 65.** (a) Temporal evolution of dimensionless HZ area for different values of Γ_d
 455 and δ (colored lines). Time-to-peak (t_p) and flood duration (t_d) are marked by vertical
 456 dashed lines.For clarity, the results for each Γ_d -condition from 0.1 to 100 are shown
 457 again separately in (b) to (e), with inserts representing smaller scales.—

458

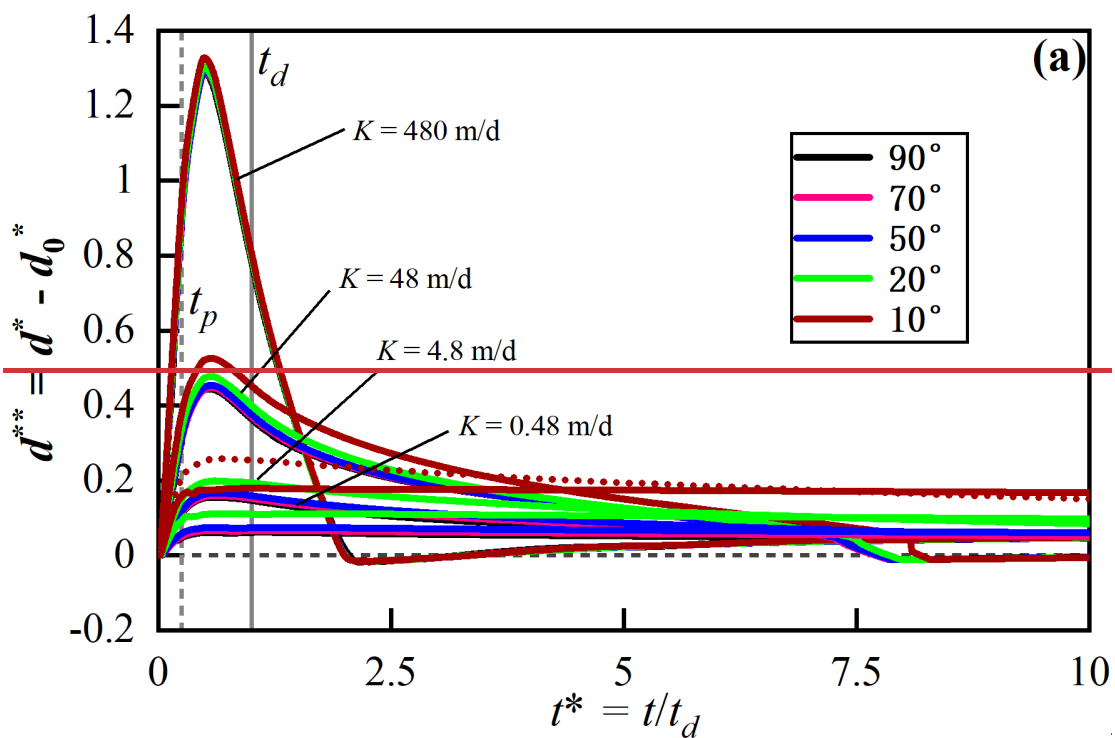


459

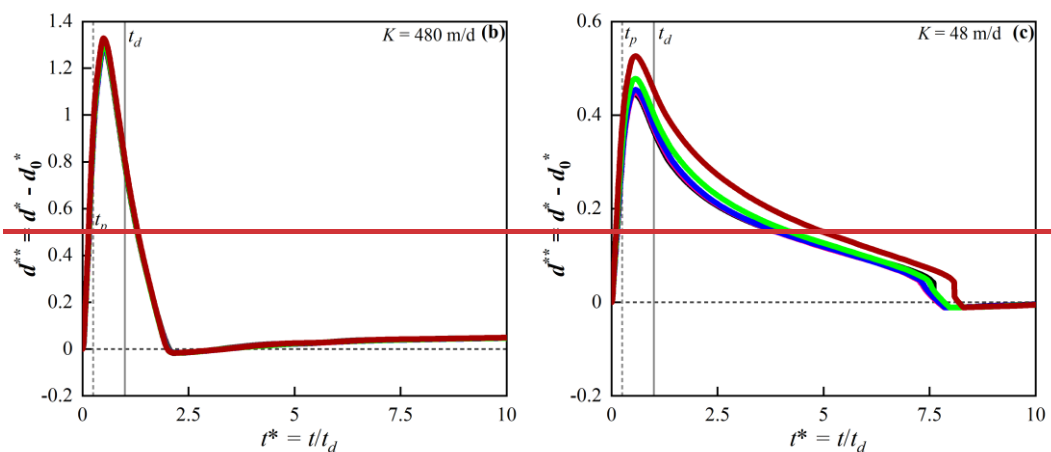
460

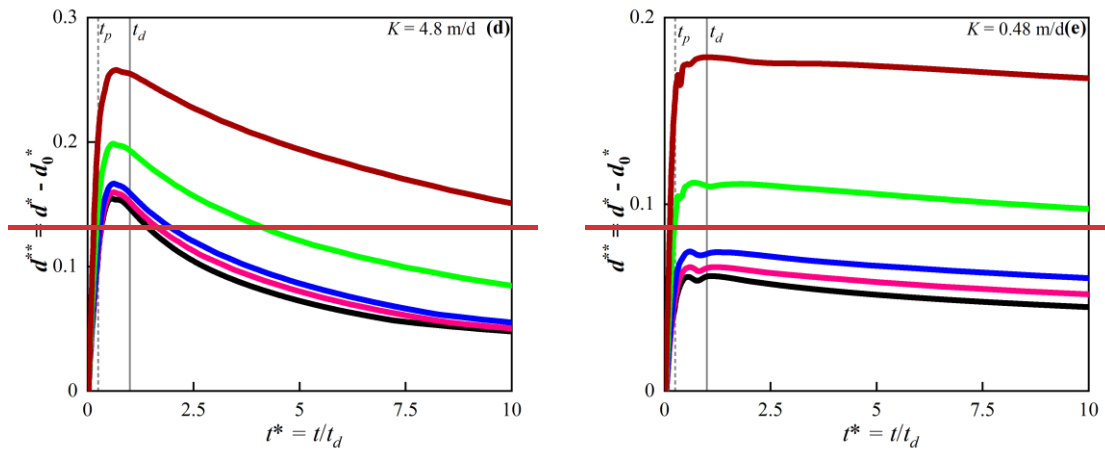


461



462





463
 464 **Figure 76.** ~~(a)~~ Temporal evolution of dimensionless HZ penetration distance into the
 465 alluvial valley (d^{**}) for alternative different values of Γ_d and δ (color lines). Time-to-
 466 peak (t_p) and flood duration (t_d) are marked by vertical dashed lines. For clarity, the
 467 results for each Γ_d -condition from 0.1 to 100 are shown again in (b) to (e), with inserts
 468 representing smaller scales.

469
 470 For vertical banks ($\delta = 90^\circ$, ~~grey-black~~ lines in Fig. 65), the $A^{**}(t)$ HZ area
 471 increases synchronously with the river stage ($t < t_p$). After the peak time of the flood
 472 event ($t > t_p$), the HZ area $A^{**}(t)$ continues to rise extend as river due to the water in the
 473 river still discharging recharges into the aquifer. Furthermore, the groundwater mound
 474 (raised water table) continues to expand, migrating into the aquifer (see the more
 475 penetrated groundwater mound from in Fig. 34b vs Fig. 34e). After the flood event ($t >$
 476 t_d), the river water that was stored in the aquifer ($C(x, t) > 0$) slowly discharges back
 477 into the river channel. Thus, the HZ area and penetration distance gradually rebound to
 478 initial conditions.

479 Under sloping riverbank conditions, the riverbank will at times be submerged by
 480 the rising river stage. Fig. 56ab and 67ab show that the effects of bank slope on HZ area
 481 ($A^{**}(t)$ in Fig. 6) and penetration distance ($d^{**}(t)$ in Fig. 7) are almost counteracted by
 482 the high transmissivity of the aquifer and the influence of bank slope ~~on HZ area and~~
 483 ~~penetration distance is was~~ negligible. At the beginning of the flood event, Fig. 56be -
 484 ~~- 56de~~ show that for conditions with smaller ~~δ sloping angle~~, $A^{**}(t)$ HZ area can be less

485 than zero (HZ at these times are smaller than the initial condition). This is due to the
 486 fact that the movement of the SWI during a rising river stage towards the alluvial valley
 487 will submerge parts that were previously unsaturated as the aquifer with low
 488 transmissivity will propagate water more slowly. As F_d aquifer transmissivity
 489 decreases from Fig. 56bd – 56de, smaller values of A^{**} were observed that the relative
 490 HZ area stay remains negative for a longer time for smaller bank slopes δ . This indicates
 491 that the bank slope has a more significant-pronounced effect on HZ area-extent in cases
 492 where F_d aquifer transmissivity is large as a low-transmissivity aquifer takes more time
 493 to propagate infiltrating river water.

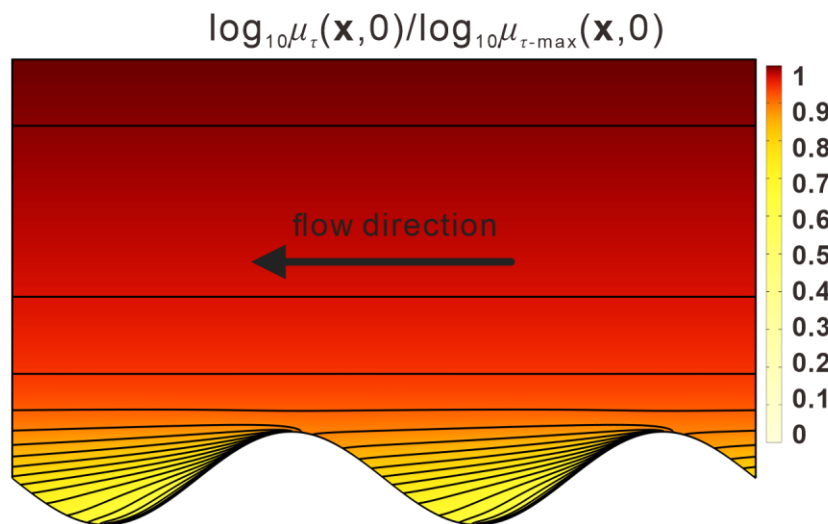
494 After about half of the flood duration ($t > 0.5t_d$), all of $A^{**}(t)$ relative HZ area the
 495 HZ area (A^{**}) becomes positive in all scenarios as due to the re-emergence of the model
 496 domain previously submerged during the flood event re-emerges. As F_d aquifer
 497 transmissivity decreases (from Fig. 56ab – 56de and from Fig. 76ab – 76d)e, the
 498 impact of bank slope δ gradually emerges-increases especially in low aquifer
 499 transmissivity-larger F_d conditions, whereby smaller bank slope δ can increase the peak
 500 values of $A^{**}(t)$ and $d^{**}(t)$ area and penetration distance of HZ, and delay the arrival
 501 time-to-peak value of the -of the maximum value of $A^{**}(t)$ relative HZ area. After the
 502 flood event ($t > t_d$), the effect of bank slope is counteracted by the higher aquifer
 503 transmissivity and only for large-lower transmissivities have a significant impact on
 504 the HZ resulting in larger $A^{**}(t)$ and $d^{**}(t)$ as shown in Fig. 56be – 56de and Fig. 67be
 505 – 67de. For low transmissivity scenarios, the bank slope can increase the peak area and
 506 penetration of HZ by almost 200%., and the lasting time of that impact positively
 507 related to the aquifer transmissivity.

508 3.2 Spatiotemporal evolution of mean residence time distribution

509 The evolution of spatiotemporal patterns of mean RTD (i.e., travel time of river
 510 water in aquifer) is a useful evaluation method for identifying the dynamic variation of
 511 aging and rejuvenation of hyporheic water. Here we use the mean RT ratio between a

512 sloping model and a vertical model $\mu_r^*(\mathbf{x}, t) = \log_{10}(\mu_{\tau-S}(\mathbf{x}, t)/\mu_{\tau-V}(\mathbf{x}, 0))$ to evaluate the
 513 influence of bank slope on the prediction of RTD for a given location and time
 514 (~~overestimates or underestimates~~). Fig. 78 presents RTDs for the initial condition,
 515 where $\mu_{\tau0-\max}$ is the maximum RT in the domain. It can be seen that the isolines
 516 representing the RT are almost horizontal in the area extending from the river but RT
 517 near the upstream river bend is smaller than downstream because the initial flow
 518 direction is towards the negative direction of the x axis. Notably, $\mu(\mathbf{x}, 0)$ grows almost
 519 exponentially as y increases, and a positive correlation to Γ_d at a given location is
 520 observed.

521



522

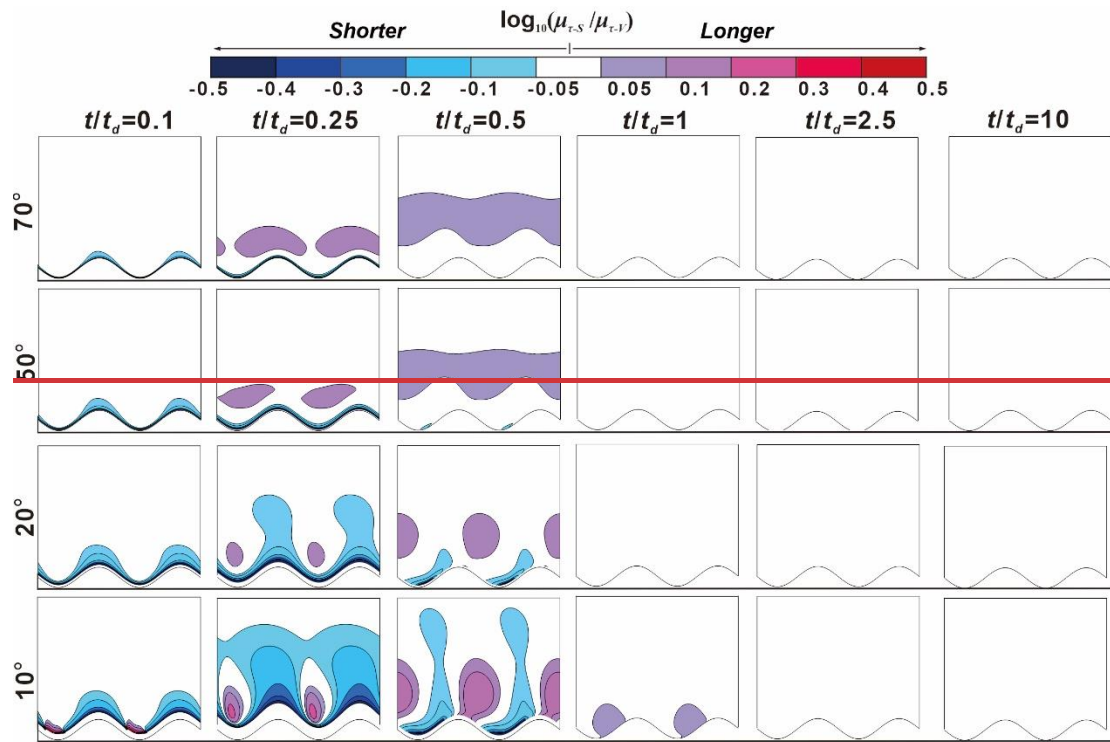
523 **Figure 78.** Relative mean residence time distributions [-] for baseline flow conditions
 524 (no bank slope), which are represented by $\log_{10}\mu_{\tau}(\mathbf{x}, 0)/\log_{10}\mu_{\tau-\max}(\mathbf{x}, 0)$ to show the
 525 distribution pattern. The value of the contour lines grows exponentially with the
 526 distance from the river meander.

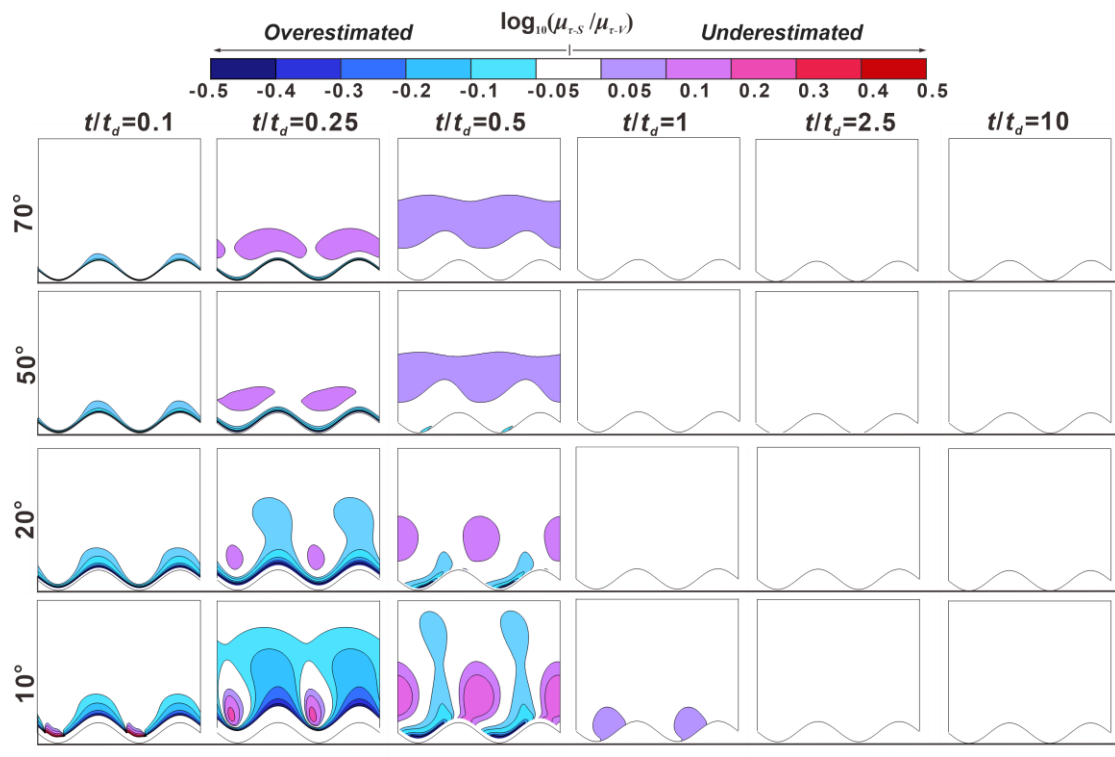
527

528 Fig. 98 - 121 present five snapshots of μ_r^* for different bank slope angles ~~for~~ and
 529 different aquifer transmissivity aquifers ($\Gamma_d = 0.1, 1, 10$ and 100 , respectively). The
 530 five snapshots represent ~~at~~ the rising limb of the flood event ($t/t_d = 0.1$), the peak of
 531 the flood event ($t/t_d = 0.25$), the falling limb of the flood event ($t/t_d = 0.5$) and a time
 532 after the flood event ($t/t_d = 1, 2.5$ and 10). The RT differences between sloping and

533 vertical riverbank models are within 12.2% in the white-colored areas ($-0.05 < \mu_r^* <$
 534 0.05) of Fig. 89 - 142, which indicates a minor effect of bank slope on RTD. The colored
 535 areas in Fig. 9 - 2412 indicate model results where neglecting bank slope in models
 536 will result will lead to an overestimated ($\mu_r^* < -0.05$) or underestimated ($\mu_r^* > 0.05$) RT
 537 prediction of residence (travel) time.

538

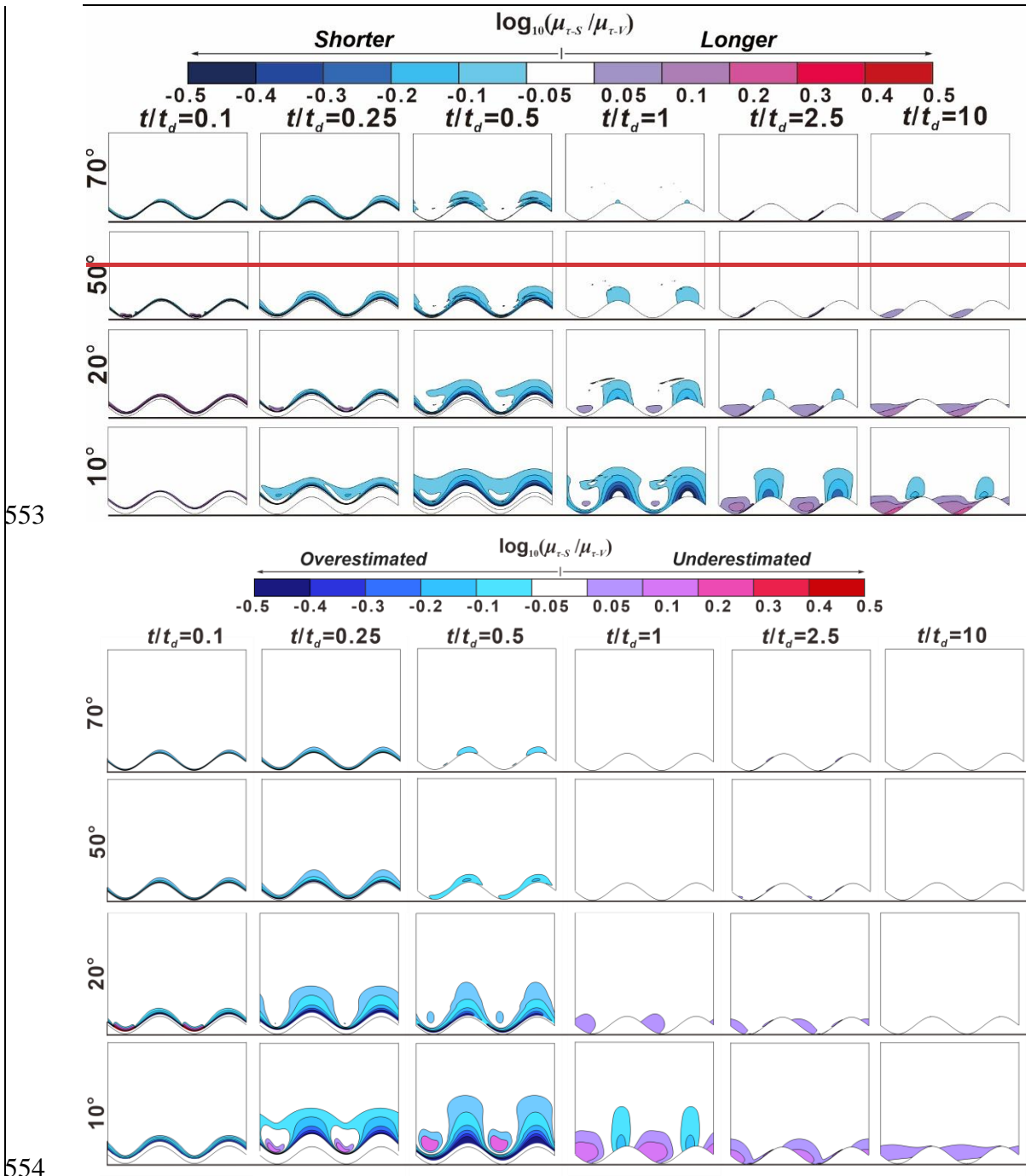




540
 541 **Figure 89.** Five snapshots for the RTD ratio $(\mu_{r-S}^*(\mathbf{x}, t) = \mu_{r-S}^*(\mathbf{x}, t) / \mu_{r-V}^*(\mathbf{x}, t))$
 542 $\mu_{r-V}^*(\mathbf{x}, t)$ between sloping $(\mu_{r-S}^*(\mathbf{x}, t))$ and vertical riverbank conditions $(\mu_{r-V}^*(\mathbf{x}, t))$ at
 543 different times t/t_d as a function of δ for $\Gamma_d = 0.1$. Warm and cold colors in Fig. 9
 544 indicates neglecting bank slope would underestimate and overestimate in the prediction
 545 of RT, respectively. The horizontal lines beneath each figure are the reference lines to
 546 show the initial location of the peak point of the SWI point bar. The lower sinuous lines
 547 at the reference lines are the initial SWIs. The colored areas indicate where the bank
 548 slopes have significant impact on RT (difference in RT between sloping and vertical
 549 models larger than 12.2%) and residence (travel) times of river water in the aquifer
 550 would be overestimated or underestimated.

551

552

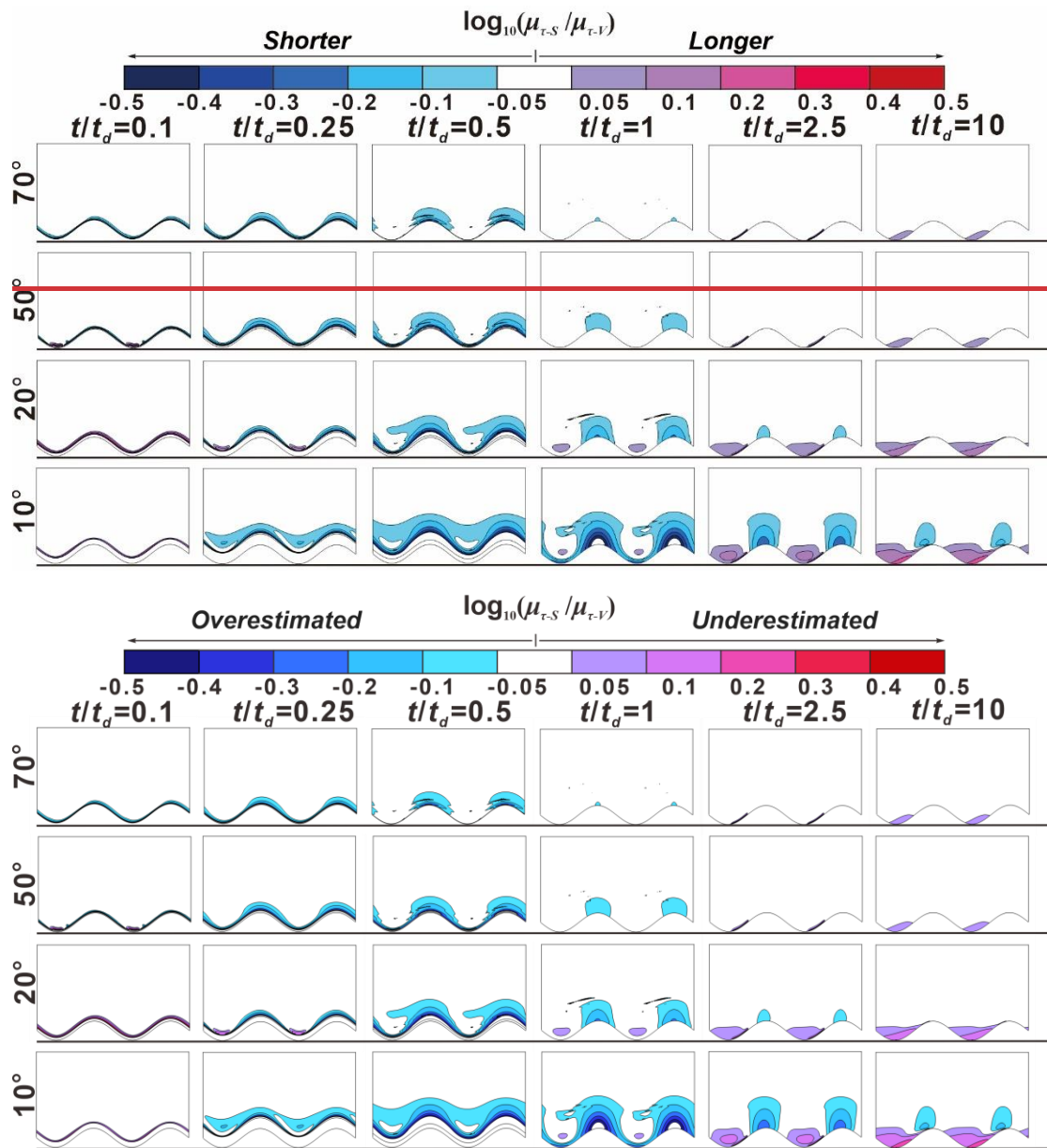


555 **Figure 910.** Five snapshots for the RTD ratio ($\mu_r^*(\mathbf{x}, t) = \mu_{r-S}^*(\mathbf{x}, t) / \mu_{r-V}^*(\mathbf{x}, t)$) between
 556 sloping ($\mu_{r-S}^*(\mathbf{x}, t)$) and vertical riverbank conditions ($\mu_{r-V}^*(\mathbf{x}, t)$) at different times t/t_d
 557 as a function of δ for $\Gamma_d = 1$. The horizontal lines beneath each figure are the reference
 558 lines to show the initial location of the peak point of the point bar. The lower sinuous
 559 lines at the reference lines are the initial SWIs. The colored areas indicate where the
 560 bank slopes have significant impact on RT (difference in RT between sloping and
 561 vertical model larger than 12.2%) and residence (travel) times of river water in the

562 aquifer would be overestimated or underestimated Snapshots for the RTD ratio $\mu_r^*(\mathbf{x}, t)$
 563 between sloping and vertical riverbank conditions at different times t/t_d as a function of
 564 δ bank slope angle for $F_d=1$. The horizontal lines beneath each figure are the reference
 565 lines to show the initial location of peak point of point barSWI. The lower sinuous lines
 566 at the reference lines are the initial SWIs. (difference in RT between sloping and vertical
 567 models larger than 12.2%).

568

569

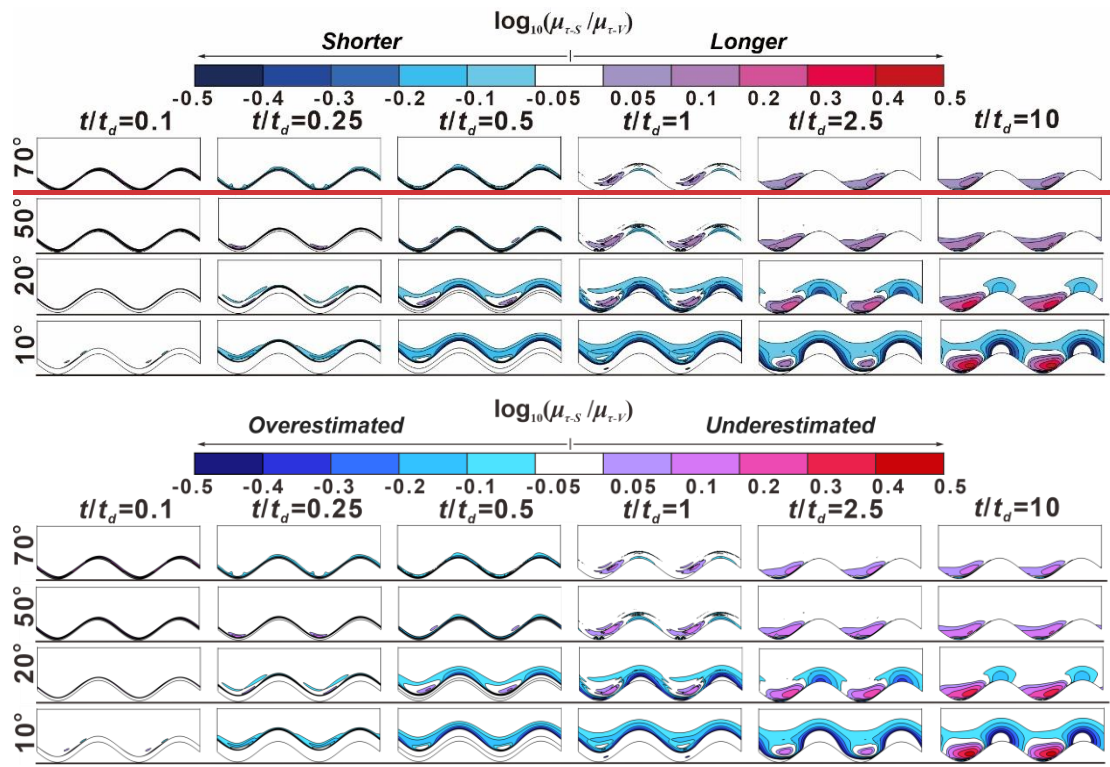


570

571 **Figure 110.** Five snapshots for the RTD ratio ($\mu_r^*(\mathbf{x}, t) = \mu_{r,S}^*(\mathbf{x}, t) / \mu_{r,V}^*(\mathbf{x}, t)$) between
 572 sloping ($\mu_{r,S}^*(\mathbf{x}, t)$) and vertical riverbank conditions ($\mu_{r,V}^*(\mathbf{x}, t)$) at different times t/t_d

573 as a function of δ for $F_d = 10$. The horizontal lines beneath each figure are the reference
 574 lines to show the initial location of the peak point of the point bar. The lower sinuous
 575 lines at the reference lines are the initial SWIs. The colored areas indicate where the
 576 bank slopes have significant impact on RT (difference in RT between sloping and
 577 vertical model larger than 12.2%) and residence (travel) times of river water in the
 578 aquifer would be overestimated or underestimated. Snapshots for the RTD ratio $\mu_r^*(x, t)$
 579 between sloping and vertical riverbank conditions at different times t/t_d as a function of
 580 bank slope angle δ for $F_d = 10$. The horizontal lines beneath each figure are the reference
 581 lines to show the initial location of SWI peak point of point bar. The lower sinuous lines
 582 at the reference lines are the initial SWIs. (difference in RT between sloping and vertical
 583 models larger than 12.2%).
 584 _____

585



586

587

588 **Figure 12.1.** Five snapshots for the RTD ratio ($\mu_r^*(\mathbf{x}, t) = \mu_{r-S}^*(\mathbf{x}, t) / \mu_{r-V}^*(\mathbf{x}, t)$) between
 589 sloping ($\mu_{r-S}^*(\mathbf{x}, t)$) and vertical riverbank conditions ($\mu_{r-V}^*(\mathbf{x}, t)$) at different times t/t_d
 590 as a function of δ for $\Gamma_d = 100$. The horizontal lines beneath each figure are the reference
 591 lines to show the initial location of the peak point of the point bar. The lower sinuous
 592 lines at the reference lines are the initial SWIs. The colored areas indicate where the
 593 bank slopes have significant impact on RT (difference in RT between sloping and
 594 vertical model larger than 12.2%) and residence (travel) times of river water in the
 595 aquifer would be overestimated or underestimated. Snapshots for the RTD ratio $\mu_r^*(\mathbf{x}, t)$
 596 between sloping and vertical riverbank conditions at different times t/t_d as a function of
 597 δ bank slope angle for $\Gamma_d = 100$. The horizontal lines beneath each figure are the
 598 reference lines to show the initial location of peak point of point bar SWI. The lower
 599 sinuous lines at the reference lines are the initial SWIs. (difference in RT between
 600 sloping and vertical models larger than 12.2%).

601

602 At $t/t_d = 0.1$, a smaller bank slope can lead to shorter RT-travel time of river water

603 in the aquifer (negative values of μ_r^*) near the SWI compared to the vertical riverbank
 604 condition scenario. The area of shorter travel time RT caused by bank slope was
 605 positively related to aquifer transmissivity. The effect of bank slope δ is small for $\Gamma_d =$
 606 10 and 100 because the groundwater mound (the raised groundwater stage) piles up
 607 around the river boundary, but that small area extended deeper into the alluvial valley
 608 for smaller δ slope angles. Due to the scattered and nested flow paths near the inner
 609 bend (cut bank) and outer bend (point bar), respectively, the penetration distance of
 610 the area of negative value of μ_r^* area at the cut bank of SWI is larger than that at the point
 611 bar. The change of flow direction near the point bar leads to a prolonged flow path for
 612 the water in the river as well as to forced groundwater mixing with the slightly older
 613 water (as shown in Fig.8 that the water was more aged in y direction compared to -x
 614 direction in the point bar). This effect was amplified with decreasing bank slope angle,
 615 but it is only statistically significant ($\mu_r^* < -0.05$ or $\mu_r^* > 0.05$) when $\delta = 10^\circ$ at $t/t_d =$
 616 0.1.

617 At the time of peak flood ($t/t_d = 0.25$), the river still infiltrates into the aquifer.
 618 For $\Gamma_d = 0.1$, Results of μ_r^* in Fig. 9 shows that bank slope can lead to both
 619 overestimated and underestimated RT area younger and older water, i.e., water
 620 undergoing shorter and longer RT. Both magnitude of relative RT (μ_r^*) and associated
 621 RT area increase with decreasing slope due to the longer penetration travel distance of
 622 river water into the aquifer. As the δ slope angle decreases, the underestimated travel
 623 time area positive values of μ_r^* are whereas located closer to the peak of the downstream
 624 point bar cut bank. The impact of bank slope on RTD for $\Gamma_d = 1$ is was rather similar in
 625 its pattern compared to $\Gamma_d = 0.1$, but μ_r^* was significant only for $\delta = 10^\circ$ the degree of
 626 that impact was reduced. For $\Gamma_d = 10$ and 100, only overestimated travel time area can
 627 be seen near the river bank with a smaller area of impact area compared to smaller Γ_d
 628 conditions, because the groundwater mounds have has not sufficiently not propagated
 629 into the aquifer in these low due to lower transmissivity aquifers.

630 the effect of bank slope can lead to larger and deeper penetration of the river water

631 ~~into the alluvial valley (Fig. 8—11) but this effect is smaller than when looking at~~
 632 ~~smaller Γ_d because of the lower hydraulic transmissivity.~~

633 At $t/t_d = 0.5$, part of the ~~submerged~~ aquifer that was submerged at $t/t_d = 0.25$
 634 reemerges due to the decline in river stage. In most cases, smaller bank slopes can lead
 635 to wider reemergence of the aquifer, ~~and which~~ therefore results in overestimated travel
 636 time area ~~smaller μ_r^*~~ near the river boundary; however, this ~~is was~~ not the case for $\Gamma_d =$
 637 0.1 where bank slope can both lead to overestimated and underestimated travel time
 638 area ~~increase and decrease the RT of pore water~~. Furthermore, compared to when $t/t_d =$
 639 0.25, the impact of bank slope becomes weaker for $\Gamma_d = 0.1$, but more relevant for the
 640 larger Γ_d values. _

641 After the flood event ($t/t_d > 1$), the influence of bank slope on ~~RT~~ travel time is
 642 nearly eliminated for $\Gamma_d = 0.1$ and 1 due to the high aquifer transmissivity. However,
 643 for aquifers with lower transmissivity ($\Gamma_d = 10$ and 100), bank slope still has a
 644 significant effect on RT at $t/t_d = 10$ and leads to underestimated and overestimated RT
 645 area ~~older water~~ near the point bar and the cut bank, respectively, ~~which indicates the~~
 646 ~~bank slope has a more lasting influence on aquifer RT, as more time is required to~~
 647 ~~recover to initial condition.~~

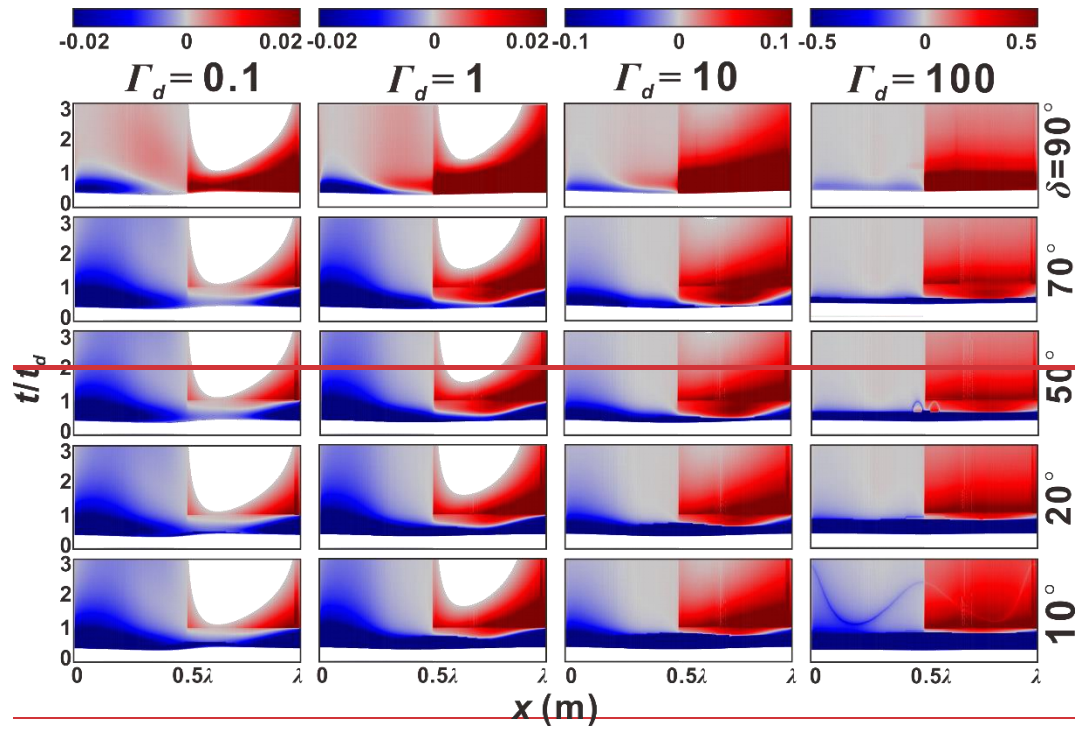
648 Overall, Fig. 9—to Fig-12 indicate that the time when bank slope was relevant in
 649 predicting RT (travel time of groundwater in aquifer) was determined by the
 650 transmissivity of aquifer. For higher transmissivity aquifer, the impact of bank slope on
 651 the prediction of groundwater travel time cannot be neglected during the flood event (0
 652 $< t < t_d$), but that impact will be eliminated after flood event due to the quickly recovery
 653 of aquifer to the base condition. For lower transmissivity aquifer, bank slope plays an
 654 important role on groundwater travel time after the half time of flood event ($t > 0.5*t_d$)
 655 and has a more lasting influence on aquifer RT, as more time is required to recover to
 656 initial condition for lower transmissivity aquifer.

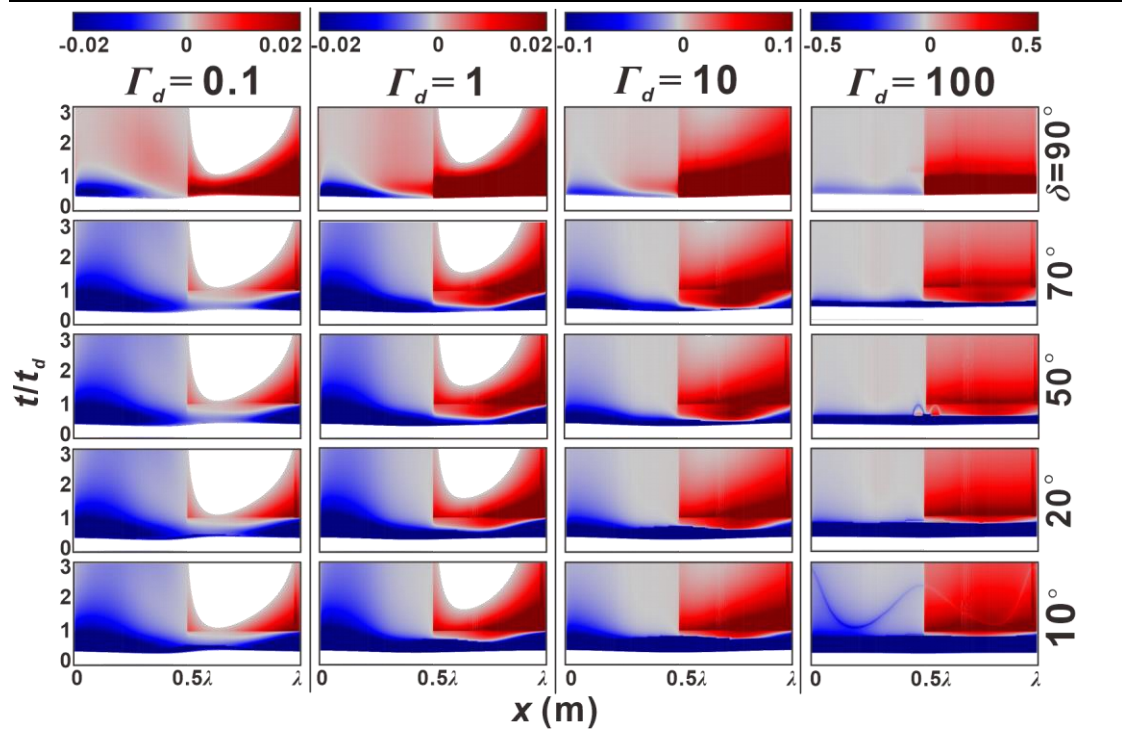
657

658 3.3 Relative flux-weighted residence time

659 Fig. 132 shows the evolution of the flux-weighted relative RT $\mu^*_{out}(x, t) = \mathbf{n} \cdot \mathbf{Q}^*_{out}(x,$
 660 $t) \log_{10}(\mu_\tau(x, t) / \mu_\tau(x, 0))$ for different slopes and aquifer transmissivities. $M^*_{out}(x, t)$
 661 represents the difference in flux-weighted RT of the water discharged into the river
 662 compared to the initial condition. At the start of the flood event, there is no μ^*_{out} as river
 663 water infiltrates the aquifer. Following the decline in river stage, the aquifer begins to
 664 discharge the mixed water with different RT back into the river (see Fig. 43c).

665





667

668 **Figure 132.** Temporal evolution of flux-weighted ratios of RT to the RT for **base**
 669 **flow** **baseline** conditions ($\mu^*_{out}(x, t) = \mathbf{n} \cdot \mathbf{Q}^*_{out}(x, t) \log_{10}(\mu_{\tau}(x, t)/\mu_{\tau}(x, 0))$) along the river
 670 meander as a function of δ and Γ_d . $\mu^*_{out}(x, t)$ indicates the difference of flux weighted
 671 water RT (travel time) that the aquifer discharges into river compared to the initial
 672 condition.

673

674 For vertical riverbank conditions ($\delta = 90^\circ$, top row in Fig. 132), upstream ($0.5\lambda <$
 675 $x < \lambda$) and downstream ($0 < x < 0.5\lambda$) boundaries of the meander bend discharge older
 676 and younger water, respectively. The rejuvenated or aged ~~with relatively younger~~
 677 ~~or older RT~~ that represent shorter and longer travel times compared to the baseline
 678 condition, respectively, are were mostly discharged before the flood event ($t/t_d < 1$) due
 679 to the greater outflux as shown in Fig. 32a. It also can be seen that water ~~is was~~ older
 680 aged along the upstream bend compared to the more rejuvenated water along the
 681 downstream bend. After the flood event, μ^*_{out} gradually disappears along the upstream
 682 meander (blank areas) for $\Gamma_d = 0.1$ and 1, because the flow fields ~~are were~~ recovering
 683 to baseline ~~flow~~ conditions. Therefore, the upstream meander gradually becomes the
 684 inflow boundary.

685 For cases with lower values of Γ_d (left columns in Fig. 132), μ^*_{out} reaches
 686 equilibrium earlier compared to cases with higher Γ_d . As δ ~~decreases from the top row~~
 687 ~~to the bottom row in Fig. 132~~, the increased impact of bank slope causes μ^*_{out} to
 688 gradually decrease the ~~RT-travel time~~ of the ~~outflowing~~ ~~water~~ during the flood event.
 689 For larger Γ_d , μ^*_{out} ~~is-was~~ totally dominated by ~~rejuvenated younger~~-water during the
 690 flood event. Furthermore, the stronger impact of smaller bank slope angles can both
 691 extend the time over which and increase the magnitude with which younger water ~~is~~
 692 ~~was~~ discharging along the downstream meander.

693 4. Discussion

694 4.1. Why we should account for bank slope

695 Tilted riverbanks are common in nature and caused by erosion and bank collapse,
 696 as has been observed at multiple scales (Zingg, 1940). Previous studies have shown that
 697 bank erosion is stronger where the river planimetry is more sinuous, river stage varies
 698 more frequently, or where the riverbank has larger sloping angles, ultimately leading to
 699 a flatter bank (Zingg. 1940; Hagorty et al., 1995; Mayor et al., 2008; Puttock et al.,
 700 2013). ~~Hence, recent studies have recognized the need for a comprehensive analysis of~~
 701 ~~how riverbank topography affects lateral hyporheic exchange along meandering~~
 702 ~~streams (Boano et al., 2014) and the specific importance of bank slope on hyporheic~~
 703 ~~exchange has been highlighted by Doble et al. (2012) and Liang et al. (2018).~~ Yet, ~~in~~
 704 ~~most previous studies~~, the impact of riverbank geometry and in particular bank slope
 705 on sinuosity-driven lateral hyporheic exchange was ignored ~~in most previous studies~~.
 706 ~~Flow was usually only considered perpendicular to the river axis, i.e., HEF in river flow~~
 707 ~~direction caused by the alluvial valley slope and river sinuosity was not considered.~~
 708 ~~However, as river planimetry can vary significantly along river corridors (Hooke, 2013;~~
 709 ~~Seminara, 2006), and the alluvial valley slope has a potentially non-negligible impact~~

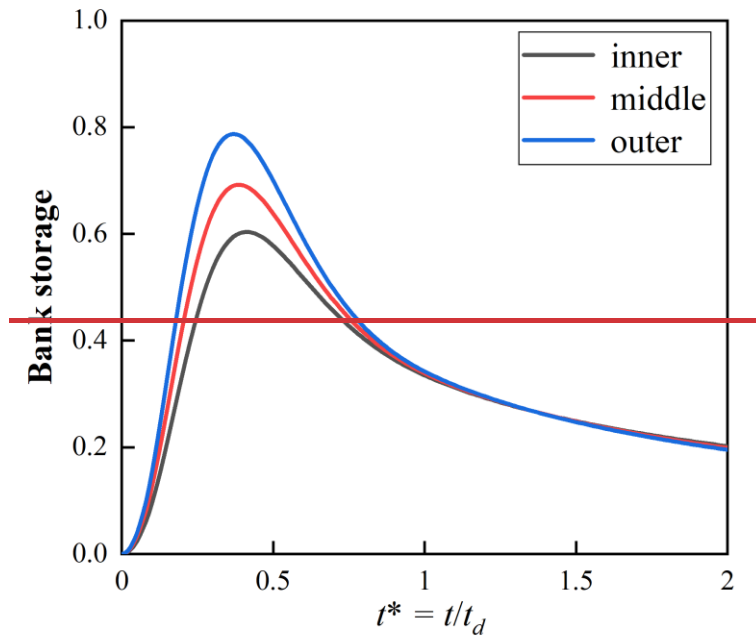
710 on hyporheic exchange (Gomez Velez et al., 2017), we considered it important to close
711 this knowledge gap by specifically focusing on the impact of bank slope and the
712 ambient groundwater gradient for various groundwater flow conditions (as manifested
713 through aquifer transmissivity) on HEF. Our results clearly indicate that HZ
714 characteristics (flow field HEF, area and penetration distance of HZ into alluvial valley)
715 can significantly be underestimated vary along a meandering river depending on bank
716 slope conditions.

717 We show that ~~N~~not accounting for bank slope and river sinuosity can lead to an
718 underestimation of the infiltration rate of water from the river to the alluvial aquifer
719 (with maximum quantity of 120% by up to 120%), as well as the area and penetration
720 distance of HZ. This effect is more pronounced for smaller bank slope angles (Fig 5),
721 and losing conditions can be significantly underestimated which can be more likely
722 found in lowland streams (Laubel et al., 2003), especially in areas with extensive cattle
723 grazing streamside (Trimble, 1994).

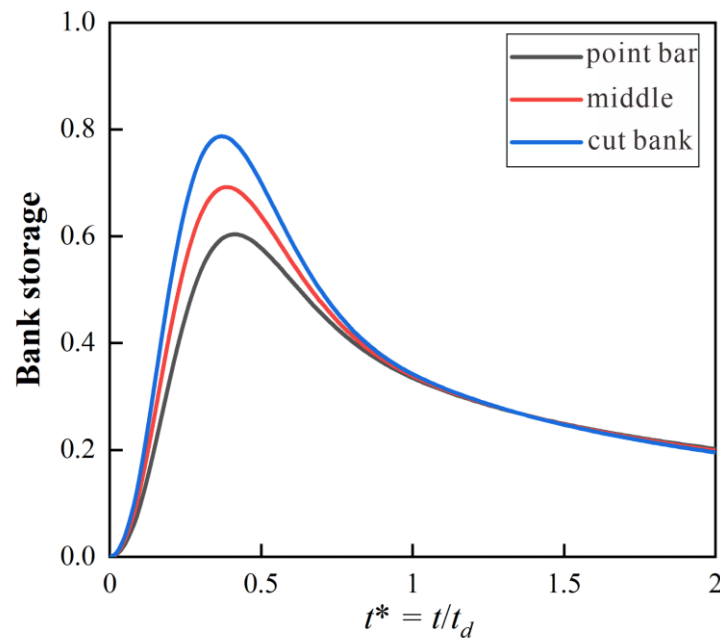
724 ~~•~~ Doble et al. (2012), Siergieiev et al. (2015) and Liang et al. (2018), assessed the
725 influence of bank slope on HEF using a vertical cross-sectional profile. Siergieiev et al.
726 (2015) found that the impact of bank slope on HEF was proportional to the hydraulic
727 conductivity of the aquifer. However, we argue here that bank slope is more relevant in
728 rivers connected to aquifers with low hydraulic transmissivity (high hydraulic
729 conductivity or low specific yield). Furthermore, we show (Fig. 14 as example³) that
730 using only one cross-sectional river profile perpendicular to the river axis does not
731 capture the effect of river sinuosity on HEF as bank storage decreases from point bar to
732 cut bank. That means This indicates ~~the previous vertical cross-sectional profile~~
733 ~~models that the accuracy of bank storage estimates can be improved could not~~
734 ~~calculate will reduce the accuracy in the calculation of the bank storage evolution~~
735 ~~accurately when by including neglecting the sinuosity of river~~ river sinuosity, which has
736 often been omitted in the past. In a meandering river with variable bank slope, river
737 geometry thus has a sizable effect on bank storage evolution and HEF, and should be

738 included in any scenarios into the future analytical/ numerical models.

739



740



741

742 **Figure 143.** Bank storage versus time for $\Gamma_d = 1$ and $\delta = 90^\circ$ condition at: inner bend
 743 peak of point bar ($x = 0$); middle bend ($x = 0.25\lambda$); outer bend peak of cut bank ($x =$

744 0.25λ). Dimensionless bank storage was calculated by $\frac{\int_{Y(x,t)}^{Y(x,t)+4\lambda} [h-z_b-H_0] dy}{\lambda H_p}$.

745

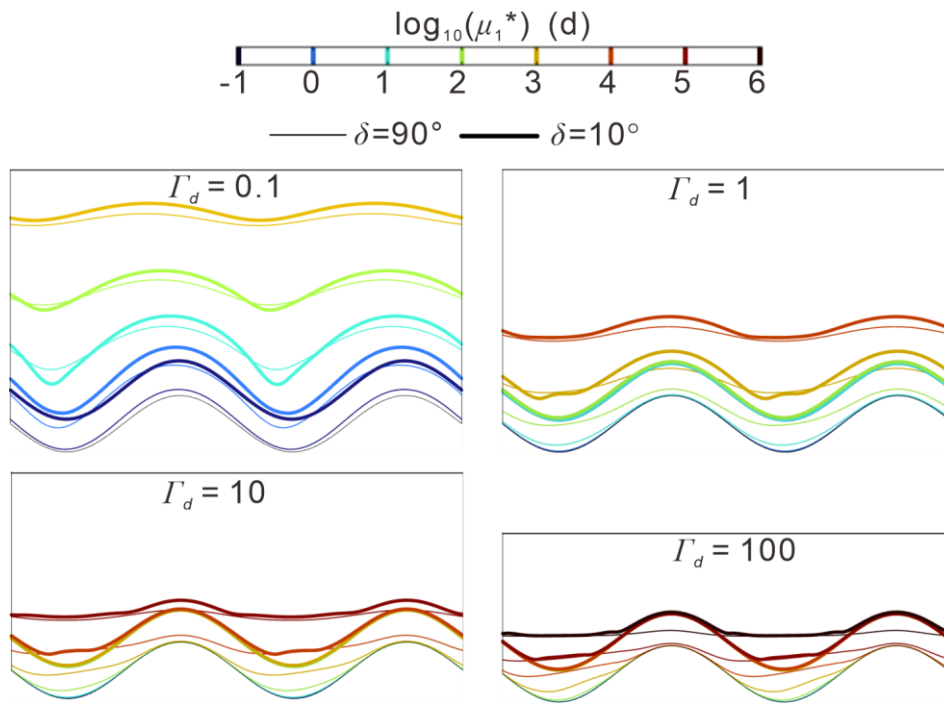
~~The impact of bank slope on RT is basically controlled by aquifer transmissivity. When aquifer transmissivity increases, the impact of bank slope appears to be more pronounced when river stage rises during a flood event. For decreasing aquifer transmissivity, bank slope seems more relevant for RTD after the flood event and its impact is more long-lasting. Bank slope could result in longer (near the point bar) or shorter (near the cut bank) pore water RT at various times of a flood event. This means that point bars with bank slopes are more conducive for river restoration (e.g., removal of dissolved organic carbon) while cut banks with bank slope may have adverse effects on the groundwater quality near rivers. This is important to keep in mind when assessing the influence of bank slope on biogeochemical efficiency. For example, previous research indicates that the residence time of river water in the HZ can control, and is often proportional to nutrient cycling (McCallum and Shanafield, 2016; Wondzell and Swanson, 1999; Zarnetske et al., 2011, 2012). As such, an analysis of RTD can provide valuable information on whether and where riverbank slope can induce biogeochemical hotspots and hot moments and help guide choices to be made in biogeochemical field surveys regarding location and sampling time under dynamic river stage conditions, especially when the connected aquifers have low hydraulic transmissivity.~~

4.2 Implications of bank slope on biogeochemical reactions

~~The impact of bank slope on RT is basically controlled by aquifer transmissivity. When aquifer transmissivity increases, the impact of bank slope appears to be more pronounced when river stage rises during a flood event. For decreasing aquifer transmissivity, bank slope seems more relevant for RTD after the flood event and its impact is more long-lasting. Bank slope could result in longer (near the point bar) or shorter (near the cut bank) pore water RT at various times of a flood event. This means~~

that point bars with bank slopes are more conducive for river restoration (e.g., removal of dissolved organic carbon) while cut banks with bank slope may have adverse effects on the groundwater quality near rivers. This is important to keep in mind when assessing the influence of bank slope on biogeochemical efficiency. For example, previous research indicates that the residence time of river water in the HZ can control, and is often proportional to nutrient cycling (McCallum and Shanafield, 2016; Wondzell and Swanson, 1999; Zarnetske et al., 2011, 2012). As such, an analysis of RTD can provide valuable information on whether and where riverbank slope can induce biogeochemical hotspots and hot moments and help guide choices to be made in biogeochemical field surveys regarding location and sampling time under dynamic river stage conditions, especially when the connected aquifers have low hydraulic transmissivity.

The RTD Residence time distributions of river water in the alluvial aquifer were widely used to evaluate the potential of biogeochemical reactions by comparing the RT with biogeochemical timescales (BTSs) for given solutes (Boano et al., 2010b; Gomez-Velez et al., 2012). The locations where the ratio of RT and to BTS is small indicate a high reaction potential for that chemical species. It has been documented that the BTS for dissolved organic matters (DOC) are site-dependent and can vary over ten⁹ orders of magnitude ($10^{-1} - 10^9$ d) (Hunter et al., 1998), while and BTSs for oxygen and nitrite have been found to vary over eight⁹ orders of magnitude ($10^{-2} - 10^6$ d) (Gomez-Velez et al., 2012). Here Thus, we compare the RTD within these two BTS ranges ($10^{-1} - 10^6$ d) between for vertical and sloping riverbank condition ($\delta = 10^\circ$) at the peak time of the flood event ($t/t_p = 0.25$) for different aquifer transmissivity conditions, and shows the zonation of residence times RT relative to the BTSs for DOC, O_2 and NO_3^- by using a BTS range of as $10^{-1} - 10^6$ d (, as shown in Fig. 15).



796

797 **Figure 15.** Zonation of biogeochemical timescales (BTS, range of $10^{-1} - 10^6$) BTSs for
 798 common HZ constituents such as reactions of DOC, oxygen and nitrate by using BTS
 799 range as $10^{-4} - 10^6$ d for different aquifer transmissivities conditions at $t/t_p = 0.25$. Thin
 800 and thick and thin colored lines indicates the results comparison of vertical vs and
 801 sloping riverbank ($\delta = 10^\circ$) conditions, respectively, while the different colors indicate
 802 the different exponents.

803

804 Fig. 15 indicates that neglecting bank slope will impact the prediction of reaction
 805 potentials of DOC, oxygen and nitrite during the hyporheic exchange process,
 806 especially for the site with short BTS locations with short time scales. For sloping bank
 807 conditions, the reaction hot areas spots (areas) expanded into the aquifer for sloping
 808 bank condition, which are identical with to the overestimated areas in Fig. 9 to Fig. 12.
 809 Note Recall that we did not aim to include specific reaction models for calculation in
 810 our study, but using RTD as an indicator for various biogeochemical reactions in the
 811 aquifer.

812

813

The impact of bank slope on RT is basically controlled by aquifer transmissivity.
 When aquifer transmissivity increases, the impact of bank slope appears to be more

814 pronounced when the river stage rises during a flood event. For decreasing aquifer
815 transmissivity, bank slope seems more relevant for RTD after the flood event and its
816 impact is more long-lasting. Bank slope could result in longer (near the point bar) or
817 shorter (near the cut bank) pore water travel times ~~at various times of~~ throughout the
818 flood event. This means that point bars with bank slopes are more ~~conducive~~ favorable
819 for ~~river restoration (e.g., removingal of~~ dissolved organic carbon and for) ~~and other~~
820 ~~oxidation reactions (e.g., nitrification)~~ while cut banks with bank slope may have
821 adverse effects on the groundwater quality near rivers. As such, an analysis of
822 ~~RTD~~ residence time distributions can provide valuable information on whether and
823 where riverbank slope can induce biogeochemical hotspots and hot moments and help
824 guide choices to be made in biogeochemical field surveys regarding location and
825 sampling time under dynamic river stage conditions, especially when the connected
826 aquifers have low hydraulic transmissivity.

827

828 **4.32. Advantages and limitations of using a reduced 2-D model**

829 In this study, we propose a parsimonious reduced-order, idealized horizontal 2-D
830 model that simplifies the variation of the river-aquifer interface by using the moving
831 boundary method to depict the displacement of the SWI along a sloping riverbank. An
832 advantage of this approach is reduced model complexity as compared to a three-
833 dimensional model, which greatly reduces time and data requirements during model
834 building and computational demand during the simulation of HEF and especially
835 residence time distributions. Thus, our reduced-order model acts as a first step to gain
836 insight into the patterns of hyporheic exchange, riverbank storage and RTD in settings
837 with more complex riverbank morphology and dynamic forcing. Future efforts should
838 be focused on optimizing the computational method applied here and on including more
839 detailed morphology and hydrodynamic characteristics.

840 ~~In It is important to note that in e~~ Our simulations we assume a constant ~~angle of~~

841 ~~bank slope~~bank slope angle along the entire meandering river while natural riverbanks
842 ~~often~~often change their slope angle from reach to reach as well as with time. This
843 ~~variability have non-uniform slopes which~~ could lead to ~~a different behavior~~more
844 complex SWI travel distances and residence time distributions and. ~~Thus,~~ new
845 conceptualizations that account for the contribution of bank slope on ~~time-varying~~time
846 varying RTD and HZ extent are needed. ~~can be applied to gain better understanding of~~
847 ~~a hyporheic zone, especially in cases where bank slope is small, or where the system is~~
848 ~~relatively insensitive to changes during peak flow.~~

849 In our simulations we tested the model using a range of aquifer hydraulic
850 conductivities. Although hydraulic conductivity (or transmissivity) is a critical
851 parameter in the quantification of exchange fluxes and RTD between the two systems
852 under varying slope conditions, other parameters such as valley water head fluctuation,
853 ~~water drinking water~~abstraction e.g. for agriculture or drinking water supply, peak
854 flood event characteristics or larger scale groundwater head fluctuation, e.g., due to
855 changing groundwater recharge patterns in the context of changing rainfall patterns have
856 not been considered here but might also impact HZ extent, RTD and river-aquifer
857 exchange flux. For example, the valley water head fluctuation and drinking water
858 abstraction in the aquifer will lead to a lower groundwater table, increasing the
859 hydraulic gradient between river and aquifer. This will lead to the formation of which
860 makes the riparian aquifer to gain water from river more easily, and form a larger area
861 of hyporheic zoneHZ area as well as a longer travel distances and times of river water
862 in the aquifer. Thus, reducing the slope of the managers should consider reducing the
863 slope of river bank could to reduce prevent the infiltration of river pollutions into
864 aquifer of polluted river water into the riparian aquifer.

865
866 The current study assumes a perennial stream and only focused on the un-confined
867 aquifer (phreatic aquifer) conditions in the connected aquifer as well as changing
868 hydraulic gradients leading to gaining and losing conditions in the river. Where there

869 is no hydraulic gradient between river and aquifer, no large-scale infiltration of river
870 water into the riverbanks will occur, while local turbulent flow (e.g., due to obstacles
871 in the river channel) might lead to localized infiltration over short distances and short
872 time scales (Sawyer et. al., 2011; Stonedahl et al., 2013; Käser et al., 2013). Where the
873 unconfined layer is small (e.g., in mountainous headwater streams with a rather small
874 sediment layer overlying a hard-rock aquifer with relatively low hydraulic
875 conductivity), the HZ is limited in its maximum extent, and travel times and distances
876 are considerably shorter. However, in mountainous settings, slope angles are often
877 much steeper due to erosion (here rivers incising into the bedrock) and further
878 simulations are required to better understand the feedback between banks slope angle,
879 hydraulic gradient and maximum extent of the unconfined layer allowing for reasonable
880 river water infiltration. These simulations will also help us better understand the impact
881 of bank slope on water supply and water quality to abstraction wells, e.g., used for the
882 production of drinking water.

883 While the using the Boussinesq equation neglects the influence of the vadose zone,
884 this approach as well as the assumption of vertically integrated distribution of hydraulic
885 head have been widely used in the literature and proven adequate when simulating
886 sinuosity-driven HEF patterns (Boano et al., 2006; 2010., Cardenas. 2008; 2009a, b;
887 Gomez-Velez et al., 2012; 2017, Kruegler et al., 2020). While we found differences in
888 HEF patterns when comparing simple models using the Boussinesq with those using
889 Richard's equation (S4 in SI) these differences exist independent of using the DGM.
890 However, we recommend in future studies to more systematically consider these two
891 different approaches with respect to their advantages and limitations, e.g., in terms of
892 computability or efficiency in predicting HEF under various conditions. While in an
893 ideal scenario a 3-D modeling approach includes vadose zone and riverbank slope angle
894 (both variable in time and space), for the moment the implementation of such detailed
895 models in practice suffers from limited computing capabilities.~~and did not address the~~
896 ~~confined condition. Because the elastic specific yield coefficient of groundwater in~~

897 ~~confined aquifer is much smaller than the gravitational one in phreatic aquifer, the~~
 898 ~~confined aquifer is expected to be more conductive for the propagation of hydraulic~~
 899 ~~pressure than phreatic aquifer. However, the SWI will be constant both in location and~~
 900 ~~length for confined aquifer, thus, we can expect that the bank slope will play non effect~~
 901 ~~on the HEF as well as RTD in confined alluvial aquifer condition.~~

902

903 5. Conclusions

904 The deformed geometry method was applied to characterize the expansion and
 905 contraction of hyporheic zones along sloping riverbanks, and to evaluate the impact of
 906 bank slope on hyporheic exchange flux, evolution of the HZ area and residence (travel)
 907 time distributions of the infiltrating waterRTD. To achieve this, several various
 908 unconfined alluvial aquifers with varying slope angles and aquifer transmissivity values
 909 were simulated. Our results show that bank slope in a sinuosity-driven river ~~can have~~
 910 ~~significant impact~~was non-negligible when the aims of numerical/analytical models are
 911 the prediction of ~~on~~ the evolution of the hyporheic zone during and after a flood event
 912 (transient flood forcing).

913 The overall findings of our work underline the need for including the assumptions
 914 of more realistic riverbank morphology morphological conditions into simulations when
 915 focus studying on the ~~a detailed analysis of~~ lateral hyporheic exchange flow responses
 916 to dynamic forcings ~~(including the assumption of more realistic riverbank morphology~~
 917 ~~conditions)~~. Furthermore, our results show that more detailed information on bank
 918 slope (e.g., through more measurements) can lead to a better understanding of
 919 hyporheic flow patterns and potentially result in improved bio~~geo~~chemical process
 920 understanding for real-world conditions ~~in~~ for more complex morphology
 921 morphological and depositional environments. Several conclusions can be drawn from
 922 our study:

- 923 1. Sloping riverbanks can considerably increase HEF during thea flood event,
 924 especially when the river is connected to an -low transmissivity alluvial aquifer
 925 with rather high hydraulic conductivity and small bank slope angles are smallas
 926 water can more easily infiltrate the connected aquifer. due to the lower ability to
 927 propagates the pressure wave and longer displacement of SWI. Smaller bank slope
 928 angles can lead to an extended hyporheic zone with river water infiltrating deeper
 929 (penetration distance) into the aquifer. -However, bank slope has only a minor
 930 impact on the hyporheic outflow flux (water re-entering the stream).
- 931 ~~2. During a flood event, the bank slope can increase the area and penetration distance~~
 932 ~~of the HZ into the alluvial aquifer. This effect increases for smaller bank slope angle~~
 933 ~~and is is more pronounced and long lasting for low transmissivity aquifers, as it~~
 934 ~~need more time to eliminates the impact of bank slope.~~
- 935 ~~3.2.~~ During a flood event, the impact of bank slope on residence time distributions (RTD)
 936 is more pronounced for high transmissivity aquifers, due to the as larger area and
 937 deeper penetration distance of the HZ forin these conditions. On the contrary, the
 938 impact of bank slope on RTD for lower transmissivity aquifers is minor during the
 939 flood event, but bank slope can have a significant and long-lasting effect under for
 940 post-flood conditions.
- 941 ~~4.3.~~ River sinuosity should be considered when assessing the impact of bank slope on
 942 RTD. Variable bank slope can lead to both longer and shorter RT-residence times
 943 when compared to vertical riverbank conditions.
- 944 ~~5.4.~~ Bank slope has a greater impact on the residence time of hyporheic water in lower-
 945 transmissivity aquifers, thereby delaying the time of younger water discharge
 946 downstream of a meander bend, which also delays the outflow of older water
 947 upstream of that bend.

948 **Code and data availability**

949 Additional information regarding methodology and results is provided in the supporting
950 information (SI).

951 **Author contributions**

952 YL: Conceptualization, Formal analysis, [Methodology](#), Investigation, [Writing](#)

953 US: Conceptualization, Methodology, Writing

954 ZW: Funding acquisition, Software, Supervision

955 SK: Validation, Writing, Supervision

956 HL: Project administration, Supervision

957 **Acknowledgements**

958 This research was partially supported by the National Natural Science Foundation of
959 China (Grant Numbers: 42272290, 41830862, and 42022018), and China Scholarship
960 Council (CSC, 202106410042).

961

962 **Competing interests**

963 The authors declare that they have no conflict of interest.

964 References

- 965 Bear, J., and Cheng, A. H. D.: Modeling groundwater flow and contaminant transport,
966 Vol. 23, pp. 83, Dordrecht: Springer, 2010.
- 967 Bertrand, G., Goldscheider, N., Gobat, J.-M., and Hunkeler, D.: Review: From multi-
968 scale conceptualization to a classification system for inland groundwater-
969 dependent ecosystems, *Hydrogeology Journal*, 20, 5-25, 2012.
- 970 Boano, F., Camporeale, C., Revelli, R., and Ridolfi, L.: Sinuosity-driven hyporheic
971 exchange in meandering rivers, *Geophysical Research Letters*, 33, L18406, 2006.
- 972 Boano, F., Harvey, J. W., Marion, A., and Packman, A. I., Revelli, R., Ridolfi, L., and
973 Wörman, A.: Hyporheic flow and transport processes: Mechanisms, models, and
974 biogeochemical implications, *Reviews of Geophysics*, 52, 603-679, 2014.
- 975 Boano, F., Demaria, A., Revelli, R., and Ridolfi, L.: Biogeochemical zonation due to
976 intrameander hyporheic flow, *Water Resource. Research.* 46, W02511, 2010.
- 977 [Boano, F., Revelli, R., and Ridolfi, L.: Effect of streamflow stochasticity on bedform-](#)
978 [driven hyporheic exchange. *Advances in Water Resources*, 33\(11\), 1367-1374.](#)
979 [2010.](#)
- 980 Boulton, A. J., Datry, T., Kasahara, T., Mutz, M., and Stanford, J. A.: Ecology and
981 management of the hyporheic zone: Stream-groundwater interactions of running
982 waters and their floodplains, *Journal of the North American Benthological Society*,
983 29 (1), 26-40, 2010.
- 984 Brunke, M., and Gonser, T.: The ecological significance of exchange processes between
985 rivers and groundwater, *Freshwater Biology*, 37 (1), 1-33, 1997.
- 986 Cardenas, M. B.: The effect of river bend morphology on flow and timescales of surface
987 water-groundwater exchange across pointbars, *Journal of Hydrology*, 362, 134-
988 141, 2008.
- 989 Cardenas, M. B.: A model for lateral hyporheic flow based on valley slope and channel
990 sinuosity, *Water Resources Research*, 45, W01501, 2009a.

-
- 991 Cardenas, M. B.: Stream-aquifer interactions and hyporheic exchange in gaining and
992 losing sinuous streams, *Water Resources Research*, 45, W06429, 2009b.
- 993 Cardenas, M. B.: Hyporheic zone hydrologic science: A historical account of its
994 emergence and a prospectus, *Water Resources Research*, 51, 3601-3616, 2015.
- 995 Cooper, H. H., and Rorabaugh, M. I.: Ground-water movements and bank storage due
996 to flood stages in surface streams, Report of Geological Survey Water-Supply, pp.
997 1536-J, US Government Printing Office, Washington, United States, 1963.
- 998 Derx, J., Farnleitner, A. H., Blöschl, G., Vierheilig, J., and Blaschke, A. P.: Effects of
999 riverbank restoration on the removal of dissolved organic carbon by soil passage
1000 during floods—A scenario analysis, *Journal of Hydrology*, 512, 195-205, 2014.
- 1001 Doble, R. C., Crosbie, R. S., Smerdon, B. D., Peeters, L., and Cook, F. J.: Groundwater
1002 recharge from overbank floods, *Water Resources Research*, 48 (9), W09522,
1003 2012a.
- 1004 Doble, R., Brunner, P., McCallum, J., and Cook, P. G.: An analysis of river bank slope
1005 and unsaturated flow effects on bank storage, *Ground Water*, 50 (1), 77-86, 2012b.
- 1006 Donea, J., A. Huerta, J.-P. Ponthot, and A. Rodriguez-Ferran.: Arbitrary Lagrangian–
1007 Eulerian methods, In *Encyclopedia of Computational Mechanics*, ed. E. Stein, R.
1008 de Borst, and T. J. R. Hughes, 413-434. New York: John Wiley & Sons, 2004.
- 1009 Duarte, F., Gormaz, R., and Natesan, S.: Arbitrary Lagrangian–Eulerian method for
1010 Navier–Stokes equations with moving boundaries, *Computer Methods in Applied
1011 Mechanics and Engineering*, 193 (45-47), 4819-4836, 2004.
- 1012 Fox, G. A., and Wilson, G. V.: The role of subsurface flow in hillslope and stream bank
1013 erosion: a review, *Soil Science Society of America Journal*, 74 (3), 717-733, 2010.
- 1014 Gao, Y., Zhu, B., Zhou, P., Tang, J. L., Wang, T., and Miao, C. Y.: Effects of vegetation
1015 cover on phosphorus loss from a hillslope cropland of purple soil under simulated
1016 rainfall: a case study in China, *Nutrient Cycling in Agroecosystems*, 85 (3), 263-
1017 273, 2009.
- 1018 Gomez-Velez, J. D., and Harvey, J. W.: A hydrogeomorphic river network model

-
- 1019 predicts where and why hyporheic exchange is important in large basins,
1020 Geophysical Research Letters, 41, 6403–6412, 2014.
- 1021 [Gomez-Velez, J. D., Wilson, J. L., and Cardenas, M. B.:](#) Residence time distributions
1022 in sinuosity-driven hyporheic zones and their biogeochemical effects, *Water*
1023 *Resources Research*, 48 (9), 2012.
- 1024 Gomez-Velez, J. D., Wilson, J. L., Cardenas, M. B., and Harvey, J. W.: Flow and
1025 residence times of dynamic river bank storage and sinuosity-driven hyporheic
1026 exchange, *Water Resources Research*, 53, 8572-8595, 2017.
- 1027 Gomez-Velez, J. D., Harvey, J. W., Cardenas, M. B., and Kiel, B.: Denitrification in the
1028 Mississippi River network controlled by flow through river bedforms, *Nature*
1029 *Geoscience*, 8, 941-945, 2015.
- 1030 Hagerty, D. J., Spoor, M. F., and Parola, A. C.: Near-bank impacts of river stage control,
1031 *Journal of Hydraulic Engineering*, 121 (2), 196-207, 1995.
- 1032 Hooke, J. M.: River meandering, In E. Wohl & J. Shroder (Eds.), *Treatise on*
1033 *geomorphology*, Vol. 9, pp. 260-288, CA: Academic Press, San Diego, 2013.
- 1034 Hester, E. T., and Gooseff, M. N.: Moving beyond the banks: Hyporheic restoration is
1035 fundamental to restoring ecological services and functions of streams,
1036 *Environmental Science and Technology*, 44 (5), 1521-1525, 2010.
- 1037 Hunt, B.: An approximation for the bank storage effect, *Water Resources Research*, 26
1038 (11), 2769–2775, 1990.
- 1039 [Hunter, K. S., Wang, Y., Van, C. P.:](#) [Kinetic modeling of microbially-driven redox](#)
1040 [chemistry of subsurface environments: coupling transport, microbial metabolism](#)
1041 [and geochemistry. *Journal of hydrology*, 209 \(1-4\), 53-80, 1998.](#)
- 1042 [Käser, D. H., Binley, A., and Heathwaite, A. L.:](#) [On the importance of considering](#)
1043 [channel microforms in groundwater models of hyporheic exchange. *River*](#)
1044 [Research and Applications](#), 29(4), 528-535, 2013.
- 1045 Kiel, B. A., Cardenas, M. B.: Lateral hyporheic exchange throughout the Mississippi
1046 River network, *Nature Geoscience*, 7 (6), 413-417, 2014.

-
- 1047 Krause, S., Abbott, B. W., Baranov, V., Bernal, S., Blaen, P., Datry, T., Drummond, J.,
1048 Fleckenstein, J. H., Gomez-Velez, J., Hannah, D. M., Knapp, J. L. A., Kurz, M.,
1049 Lewandowski, J., Marti, E., Mendoza-Lera C., Milner, A., Packman, A., Pinay, G.,
1050 Ward, A. S., Zarnetzke, J. P.: Organizational principles of hyporheic exchange flow
1051 and biogeochemical cycling in river networks across scales, *Water Resources*
1052 *Research*. 58, e2021WR029771, 2022.
- 1053 Krause, S., Hannah, D. M., Fleckenstein, J. H., Heppell, C. M., Pickup, R., Pinay, G.,
1054 Robertson, A. L., and Wood, P. J.: Inter-disciplinary perspectives on processes in
1055 the hyporheic zone, *Ecohydrology Journal*. 4 (4), 481-499, 2011.
- 1056 Krause, S., Lewandowski, J., Grimm, N., Hannah, D. M., Pinay, G., Turk, V., Argerich,
1057 A., Sabater, F., Fleckenstein, J., Schmidt, C., Battin, T., Pfister, L., Martí, E.,
1058 Sorolla, A., Larned, S., and Turk, V.: Ecohydrological interfaces as critical
1059 hotspots for ecosystem functioning, *Water Resources Research*. 53, 6359-6376,
1060 2017.
- 1061 Krause, S., Tecklenburg, C., Munz, M., and Naden, E.: Streambed nitrogen cycling
1062 beyond the hyporheic zone: Flow controls on horizontal patterns and depth
1063 distribution of nitrate and dissolved oxygen in the upwelling groundwater of a
1064 lowland river, *Journal of Geophysical Research: Biogeosciences*, 118 (1), 54-67,
1065 2013.
- 1066 Kruegler, J., Gomez-Velez, J. D., Lautz, L. K., and Endreny, T. A.: Dynamic
1067 evapotranspiration alters hyporheic flow and residence times in the intrameander
1068 zone, *Water*, 12 (2), 424, 2020.
- 1069 Larkin, R. G., and Sharp, J. M.: On the relationship between river-basin geomorphology,
1070 aquifer hydraulics, and groundwater flow direction in alluvial aquifers, *Geological*
1071 *Society of America Bulletin*, 104, 1608-1620, 1992.
- 1072 Laubel, A., Kronvang, B., Hald, A. B., and Jensen, C.: Hydromorphological and
1073 biological factors influencing sediment and phosphorus loss via bank erosion in
1074 small lowland rural streams in Denmark. *Hydrological processes*, 17(17), 3443-

- 1075 [3463, 2003.](#)
- 1076 Li, H., Boufadel, M. C., and Weaver, J. W.: Quantifying bank storage of variably
1077 saturated aquifers, *Ground Water*, 46 (6), 841-850, 2008.
- 1078 Liang, X. Y., Zhan, H. B., and Schilling, K.: Spatiotemporal responses of groundwater
1079 flow and aquifer-river exchanges to flood events, *Water Resources Research*, 54
1080 (3), 1513-1532, 2018.
- 1081 Lindow, N., Fox, G. A., and Evans, R. O.: Seepage erosion in layered stream bank
1082 material, *Earth Surface Processes and Landforms*, 34 (12), 1693-1701, 2009.
- 1083 Mayor, Á. G., Bautista, S., Small, E. E., Dixon, M., and Bellot, J.: Measurement of the
1084 connectivity of runoff source areas as determined by vegetation pattern and
1085 topography: A tool for assessing potential water and soil losses in drylands, *Water
1086 Resources Research*, 44 (10), 2008.
- 1087 Maury, B.: Characteristics ALE method for the unsteady 3D Navier-Stokes equations
1088 with a free surface, *International Journal of Computational Fluid Dynamics*, 6 (3),
1089 175-188, 1996.
- 1090 McCallum, J.L., P.G. Cook, P. Brunner, and D, Berhane.: Solute dynamics during bank
1091 storage flows and implications for chemical baseflow separation, *Water Resources
1092 Research*, 46: W07541, 2010.
- 1093 McClain, M. E., Boyer, E. W., Dent, C. L., Gergel, S. E., Grimm, N. B., Groffman, P.
1094 M., Hart, S. C., Harvey, J. W., Johnston, C. A., Mayorga, E., Mcdowell, W and
1095 Pinay, G.: Biogeochemical hot spots and hot moments at the interface of terrestrial
1096 and aquatic ecosystems, *Ecosystems*, 6 (4), 301-312, 2003.
- 1097 Millar, R. G., and Quick, M. C.: Effect of bank stability on geometry of gravel rivers,
1098 *Journal of Hydraulic Engineering*, 119 (12), 1343-1363, 1993.
- 1099 Millington, R. J., and Quirk, J. P.: Permeability of porous solids, *Transactions of the
1100 Faraday Society*, 57, 1200-1207, 1961.
- 1101 Osman, A. M., and Thorne, C. R.: Riverbank stability analysis. I: Theory, *Journal of
1102 Hydraulic Engineering*, 114 (2), 134-150, 1988.

-
- 1103 Pinay, G., Peiffer, S., De Dreuzy, J. R., Krause, S., Hannah, D. M., Fleckenstein, J. H.,
1104 Sebilo, M., Bishop, K., and Hubert-M, L.: Upscaling nitrogen removal capacity
1105 from local hotspots to low stream orders' drainage basins, *Ecosystems*, 18 (6),
1106 1101-1120, 2015.
- 1107 Pohjoranta, A., and Tenno, R.: Implementing surfactant mass balance in 2D FEM–ALE
1108 models, *Engineering with Computers*, 27 (2), 165-175, 2011.
- 1109 Puttock, A., Macleod, C. J., Bol, R., Sessford, P., Dungait, J., and Brazier, R. E.:
1110 Changes in ecosystem structure, function and hydrological connectivity control
1111 water, soil and carbon losses in semi-arid grass to woody vegetation transitions,
1112 *Earth Surface Processes and Landforms*, 38 (13), 1602-1611, 2013.
- 1113 Seminara, G.: Meanders, *Journal of Fluid Mechanics*, 554, 271-297, 2006.
- 1114 Schmadel, N. M., A. S. Ward, C. S. Lowry, and J. M. Malzone.: Hyporheic exchange
1115 controlled by dynamic hydrologic boundary conditions, *Geophysical Research*
1116 *Letters*, 43, 4408-4417, 2016.
- 1117 Sawyer, A. H., Bayani Cardenas, M., and Buttles, J.: Hyporheic exchange due to
1118 channel-spanning logs. *Water Resources Research*, 47(8), 2011.
- 1119 Sharp, J. M.: Limitations of bank-stoppage model assumptions, *Journal of Hydrology*,
1120 35 (1-2), 31-47, 1977.
- 1121 Siergieiev, D., Ehlert, L., Reimann, T., Lundberg, A., and Liedl, R.: Modelling
1122 hyporheic processes for regulated rivers under transient hydrological and
1123 hydrogeological conditions, *Hydrology and Earth System Sciences*, 19 (1), 329-
1124 340, 2015.
- 1125 Singh, T., Gomez-Velez, J. D., Wu, L., Wörman, A., Hannah, D. M., and Krause, S.:
1126 Effects of successive peak flow events on hyporheic exchange and residence times,
1127 *Water Resources Research*, 56 (8), e2020WR027113, 2020.
- 1128 Singh, T., Wu, L., Gomez-Velez, J. D., Lewandowski, J., Hannah, D. M., Krause, S.:
1129 Dynamic hyporheic zones: Exploring the role of peak flow events on bedform-
1130 induced hyporheic exchange, *Water Resources Research*, 55, 218-235, 2019.

-
- 1131 Stonedahl, S. H., Harvey, J. W., and Packman, A. I.: Interactions between hyporheic
1132 flow produced by stream meanders, bars, and dunes, *Water Resources Research*,
1133 49, 5450-5461, 2013.
- 1134 [Trimble, S. W.: Erosional effects of cattle on streambanks in Tennessee, USA. *Earth*](#)
1135 [*surface processes and landforms*, 19\(5\), 451-464, 1994.](#)
- 1136 Triska, F. J., Kennedy, V. C., Avanzino, R. J., Zellweger, G. W., and Bencala, K. E.:
1137 Retention and transport of nutrients in a third - order stream in northwestern
1138 California: Hyporheic processes, *Ecology*, 70 (6), 1893-1905, 1989.
- 1139 [Van Genuchten, M. T.: A closed - form equation for predicting the hydraulic](#)
1140 [conductivity of unsaturated soils. *Soil science society of America journal*, 44\(5\),](#)
1141 [892-898, 1980.](#)
- 1142 Weatherill, J. J., Atashgahi, S., Schneidewind, U., Krause, S., Ullah, S., Cassidy, N.,
1143 and Rivett, M. O.: Natural attenuation of chlorinated ethenes in hyporheic zones:
1144 A review of key biogeochemical processes and in-situ transformation potential,
1145 *Water research*, 128, 362-382, 2018.
- 1146 Wondzell, S. M., and Swanson, F. J.: Floods, channel change, and the hyporheic zone,
1147 *Water Resources Research*, 35 (2), 555-567, 1999.
- 1148 Wu, L., Gomez-Velez, J. D., Krause, S., Singh, T., Wörman, A., and Lewandowski, J.:
1149 Impact of flow alteration and temperature variability on hyporheic exchange,
1150 *Water Resources Research*, 56 (3), e2019WR026225, 2020.
- 1151 Wu, L., Gomez-Velez, J. D., Krause, S., Wörman, A., Singh, T., Nützmann, G., and
1152 Lewandowski, J.: How daily groundwater table drawdown affects the diel rhythm
1153 of hyporheic exchange, *Hydrology and Earth System Sciences*, 25 (4), 1905-1921,
1154 2021.
- 1155 Wu, L., Singh, T., Gomez-Velez, J. D., Nützmann, G., Wörman, A., Krause, S., and
1156 Lewandowski, J.: Impact of dynamically changing discharge on hyporheic
1157 exchange processes under gaining and losing groundwater conditions, *Water*
1158 *Resources Research*, 54 (12), 10-076, 2018.

-
- 1159 Zarnetske, J. P., Haggerty, R., Wondzell, S. M., and Baker, M. A.: Dynamics of nitrate
1160 production and removal as a function of residence time in the hyporheic zone,
1161 Journal of Geophysical Research, 116, G01025, 2021.
- 1162 Zarnetske, J. P., Haggerty, R., Wondzell, S. M., Bokil, V. A., and González-Pinzón, R.:
1163 Coupled transport and reaction kinetics control the nitrate source-sink function of
1164 hyporheic zones, Water Resources Research, 48, W11508, 2012.
- 1165 Zingg, A. W.: Degree and length of land slope as it affects soil loss in run-off,
1166 Agricultural Engineering, 21, 59-64, 1940.
- 1167